REPORT NO. HE-150-114

TECHNICAL REPORT

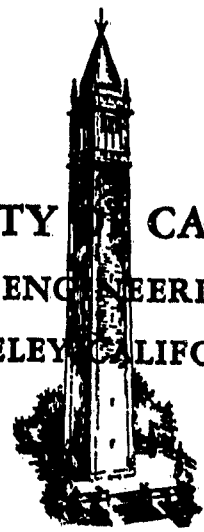

UNIVERSITY OF CALIFORNIA
INSTITUTE OF ENGINEERING RESEARCH
BERKELEY, CALIFORNIA

CONE DRAG IN A RAREFIED GAS FLOW

by

D. C. IPSEN

SERIES NO. 20

ISSUE NO. 95

DATE AUGUST 10, 1953

CONTRACT N7-onr-295-Task 3
PROJECT NR 061-003
REPORT NO. HE-150-114
SERIES NO. 20-95
AUGUST 10, 1953

JOINTLY SPONSORED BY
OFFICE OF NAVAL RESEARCH AND
OFFICE OF SCIENTIFIC RESEARCH

FLUID FLOW AND HEAT TRANSFER AT LOW PRESSURES AND TEMPERATURES

CONE DRAG IN A RAREFIED GAS FLOW

By

D. C. IPSEN

FACULTY INVESTIGATOR:

S. A. SCHAAF, ASSOCIATE PROFESSOR OF ENGINEERING SCIENCES

Approved by: S A Schaaf

ABSTRACT

Total drag on the fore portion of a 15° half-angle cone is investigated in a rarefied air flow. The principal effort was directed toward development of a compact, remote balance satisfactory for measurement of the small forces involved. The resulting design gives sufficient accuracy for the present range of forces investigated, but extension of the investigation to lower Reynolds number may require design refinement.

Tests were performed at nominal Mach numbers of 2 and 4, over corresponding ranges of free-stream Reynolds number based on cone slant length of about 150-1500 and 1000-7000. For most of this range of variables, that part of the drag due to viscous effects is greater than the inviscid wave drag. The viscous drag includes not only shear drag but also an appreciable drag component arising from the influence of viscosity on the pressure distribution. Results indicate that the viscous drag is 10 to 30 per cent greater than first-order boundary-layer predictions.

CONTENTS

NOMENCLATURE

A_f frontal area = $\pi L^2 \sin^2\alpha$

A_s surface area = $\pi L^2 \sin\alpha$

C_D drag coefficient = $\dfrac{D}{q_1 A_f}$

C_{Di} inviscid drag coefficient

C'_{Df} shear drag coefficient (theoretical)

C'_{Dp} pressure drag coefficient (theoretical)

C_F force coefficient = $\dfrac{F}{q_1 A_f}$

c_p specific heat at constant pressure

C_{pc} cone pressure coefficient = $\dfrac{p_c}{q_1}$

C_{pci} inviscid cone pressure coefficient = $\dfrac{p_{ci}}{q_1}$

D drag force = $\displaystyle\int_{A_s} \tau_x \, dA \cos\alpha + \int_{A_s} (p_x - p_1) \, dA \sin\alpha = F + (p_c - p_1) A_f$

f tangent-cone pressure parameter (defined in Appendix D)

F measured force

K_{ci} cone boundary-layer Knudsen number = $\dfrac{1.5 \, M_{ci}}{R_{ci}/L}$

k thermal conductivity

l arbitrary length (Appendix E)

L slant length of cone

LIST OF FIGURES AND TABLES

NOMENCLATURE

A_f frontal area = $\pi L^2 \sin^2\alpha$

A_s surface area = $\pi L^2 \sin\alpha$

C_D drag coefficient = $\frac{D}{q_1 A_f}$

C_{Di} inviscid drag coefficient

C'_{Df} shear drag coefficient (theoretical)

C'_{Dp} pressure drag coefficient (theoretical)

C_F force coefficient = $\frac{F}{q_1 A_f}$

c_p specific heat at constant pressure

C_{pc} cone pressure coefficient = $\frac{p_c}{q_1}$

C_{pci} inviscid cone pressure coefficient = $\frac{p_{ci}}{q_1}$

D drag force = $\int_{A_s} \tau_x dA \cos\alpha + \int_{A_s} (p_x - p_1) dA \sin\alpha = F + (p_c - p_1) A_f$

f tangent-cone pressure parameter (defined in Appendix D)

F measured force

K_{ci} cone boundary-layer Knudsen number = $\frac{1.5\, M_{ci}}{R_{ci}/L}$

k thermal conductivity

l arbitrary length (Appendix E)

L slant length of cone

M_1 free-stream Mach number

M_{ci} cone Mach number from inviscid theory

p_o stagnation pressure

p_1 free-stream pressure

p_c measured cone (housing) pressure

p_{ci} pressure at cone surface from inviscid theory

p_x local cone pressure

q_1 free-stream dynamic pressure = $\frac{1}{2}\rho_1 V_1^2$

q_{ci} dynamic pressure at cone surface from inviscid theory = $\frac{1}{2}\rho_{ci} V_{ci}^2$

r cone radius

R_1 free-stream Reynolds number (based on L)

R_{ci} Reynolds number from inviscid solution for p_{ci}, T_{ci}, M_{ci} (based on L)

R_x local R_{ci} (based on x)

T_o stagnation temperature, absolute

T_1 free-stream temperature, absolute

T_{ci} temperature at cone surface from inviscid theory, absolute

u x-component of velocity

u_x wall (slip) velocity

v	y-component of velocity
V_1	free-stream velocity
V_{ci}	velocity at cone surface from inviscid theory
x	distance along cone from tip
y	distance normal to cone surface
α	cone half-angle
β	tangent-cone half-angle (see Figure 10)
γ	specific heat ratio (1.40)
δ^*	displacement thickness of boundary layer (theoretical)
ϵ	slip coefficient (defined in Appendix E)
θ	boundary-layer slope in x-y plane (see Figure 10)
μ	absolute viscosity
ρ_1	free-stream density
ρ_{ci}	density at cone surface from inviscid theory
σ	Prandtl number
τ_x	local cone shear stress
ω	viscosity exponent

Report No. HE-150-114

CONE DRAG IN A RAREFIED GAS FLOW

1.0 INTRODUCTION

The problem of drag on the fore portion of a cone has already received attention in studies of normal-density gas flow and in studies of highly-rarefied free-molecule flows. In the intermediate slip-flow regime, however, information on cone drag has been almost completely absent. What little information there was consisted of theoretical fragments that might be pieced together from the analyses of Lin, Schaaf and Sherman (Ref. 1) and Drake and Maslach (Ref. 2) to provide a rough estimate of cone drag in this intermediate regime.

The present tests are intended to supply empirical drag information for these flows, as well as to provide possible clues to the theoretical formulation of the flow problem. The tests fall in what is usually termed the slip-flow regime. The mean free path of the gas adjacent to the cone surface ranges from 10 to 15 percent of the calculated displacement thickness of the boundary layer at the base of the cone. The flows are therefore closer to normal-density flows, where the mean free path is much smaller than any significant body or boundary-layer dimension, than to free-molecule flows, where the mean free path is much larger than any significant dimension. Comparable slip conditions could be obtained at normal densities only by test of a model of the order of a few ten thousands of an inch long.

Besides the presence of slip and associated rarefaction phenomena, the probability of appreciable interaction between the boundary layer and the free stream also serves to distinguish the present flow regime from normal-density flows, where interactions are unimportant except at hypersonic velocities. The low density of the present tests gives rise to low Reynolds numbers and thick boundary layers, which, coupled with a supersonic free stream, suggest the possibility of significant interactions. The calculated displacement thickness of the boundary layer builds up to as much as about 0.02 inches at a point

two inches from the cone tip.

Information on cone drag in the flow range investigated has practical application to flight at high altitudes. The pressure level of the tests correspond to around 30 miles elevation; however, the results provide a description of the drag on only the first couple inches of the cone at such an altitude, and are therefore of most value for flight at somewhat higher altitudes, where the reduction in density gives larger corresponding lengths at the same Reynolds number.

Perhaps of greater value that its direct application is the potential use of information on cone drag in the general development of viscous- and slip-flow theory. Of the various configurations exhibiting some susceptibility to mathematical analysis, the cone is one of the easiest to approximate experimentally. The flat plate, though more popular with the analyst, is difficult to simulate in the wind tunnel: finite thickness and aspect ratio introduce uncertainties, or at least unwanted variables, and the problem of measuring local pressure or temperature is likely to be difficult. These complications are not present for the cone.

Despite its advantages, the cone does have problems of its own. One of the most serious arises in drag measurement, where it is desired to measure the force on a portion of the cone. To keep the effect of the resulting gap between the parts negligible, the gap width must be narrow, and decrease in gap width with drag must be small. Also, the pressure within the model must be at or near the cone surface pressure in the vicinity of the gap. Otherwise, flow through the gap would distort the external flow, as well as complicate the problem of determining the internal force.

These considerations suggested the use of a force-sensing unit enclosed within the model body. A variable-reluctance unit made by the Wiancko Engineering Company, capable of detecting deflections of the order of one-millionth of an inch, was chosen as the force-sensing unit, since it enabled model deflection to be held to a small value without remote positioning. Enclosure of the unit

within the model housing permitted maintenance of cone surface pressure within the housing.

Photographs and sketches of the models and balance used are shown in Figures 1, 2 and 3. The basic cone has a slant length of 3.70 inches and a vertex half-angle of 15°. The drag model shown in these figures constitutes the forward inch of the cone. A model constituting the forward two inches was also tested. The models were supported so that their axial motion was essentially restrained only by the Wiancko unit. The drag force, less the internal pressure force on the model, thus acted directly to deflect the Wiancko armature, which is elastically supported. The attendant reluctance changes of the Wiancko unit were detected by the circuit shown in Figure 4. The d-c bridge circuit shown in this figure was used to measure the resistance of the Wiancko coils which provided an indication of the temperature within the housing. Additional description of the apparatus is included in Appendix A.

Primary calibration of the balance was accomplished by calibration of the Wiancko unit alone, using gram weights. A typical calibration, covering the force range encountered with the one-inch model, is shown in Figure 5. Because of the large zero shift caused by temperature change (nearly 2 mg per °F), calibration was performed at several temperatures and corrected to a standard value. A secondary calibration was performed with the model in place in the tunnel by applying weights to the calibration arm (Figure 3, Part 10), access to which was possible by removal of the plug in the bottom of the housing. The chief function of the latter calibration was to determine the temperature sensitivity of the supporting structure so that test readings could be corrected to the standard temperature. It also served to check possible mechanical interference with the moving parts.

Tests were made using two nozzles giving Mach numbers of approximately 2 and 4. Force and pressure measurements were taken over a range of tunnel pressure of 50 to 180 microns Hg. absolute in the Mach 2 nozzle and 50 to 140 in the Mach 4 nozzle. Appendix

A includes a brief description of the experimental apparatus. Details of the calibration and testing techniques are included in Appendix B. Reduction of data is discussed in Appendix C.

2.0 DESCRIPTION OF RESULTS

The final results are shown in Figure 6. The upper curves are the measured drag coefficients, shown compared to theoretical curves derived from boundary-layer analysis. The latter curves are discussed in Section 4.0. Although different in magnitude, the theoretical and experimental curves display similar trends and comparable Mach-number dependence. Because of the variation of Mach number with Reynolds number in each nozzle, each of the four model-nozzle combinations gives separate curves, though, apparently by coincidence, the curves for the Mach 2 nozzle fall on top of one another. In each of the nozzles the Mach number increases about ten per cent from lowest to highest flow rate. The increase arises from the change in effective area ratio caused by the thinning of the nozzle boundary layer as the Reynolds number increases.

The lower curves of Figure 6 are corrected to constant Mach number. The technique of correction is explained in Appendix D. It is based on the Mach-number dependence indicated by the theoretical boundary-layer curve. All of the curves of Figure 6 pertain to the total drag, which includes the axial component of the pressure force (relative to free-stream pressure) as well as the axial component of the shear force.

The results are presented in an alternative form in Figure 7, which shows the drag due to viscous influences. This drag is equal to the difference between the total drag and the inviscid drag, and can be interpreted as the sum of the shear drag and the increment of pressure drag caused by viscosity. The pressure-drag increment arises from interaction between the cone boundary layer and the external flow, and can be associated with the alteration in the effective shape of the cone by addition of the boundary layer. Presentation of the data in this form makes comparison with theory simpler.

The pressure measured within the housing is presented in Figure 8. Ideally this pressure is equal to the cone surface pressure at the gap. Actually it probably differs somewhat because of imperfect gap alignment. This conclusion is based primarily on the absence of a simple explanation for the deviations between theory and experiment seen in the figure. The consistent deviations seen in the drag curves are not present here. Unfortunately, gap effects are hard to distinguish from Mach-number effects. At a particular Reynolds number the two curves for a particular nozzle represent not only different models (hence gaps) but also different Mach numbers. The apparent failure of the measured cone pressure to match the surface pressure is evidently not a manifestation of large disturbances in the external flow near the gap, for the drag results show no irregularities that can be easily traced to the gap. The chief drawback in the pressure discrepancy is that it makes separate determination of the components of shear and pressure drag impossible. It is doubtful, however, that even accurate knowledge of the gap pressure would provide a complete enough pressure picture, since the evaluation of the pressure drag would require extrapolation of this information to the cone tip, i.e., to a Reynolds number of zero.

Figure 9 shows the variation of force on the model. Beyond being one of the measured ingredients of the drag, the curves have little significance. The sum of the force coefficient C_F and the cone pressure coefficient C_{pc} of Figure 8, minus the free-stream pressure coefficient p_1/q_1, is equal to the total drag coefficient. Had the viscous pressure drag been negligible and had the measured cone pressure matched the surface pressure, the force coefficient would have been identical to the shear drag coefficient. Since the first requirement is almost certainly not met, and the second also unlikely to be met, the force coefficient has little or no significance by itself, except to indicate the internal consistency of the data.

The results are also tabulated in Tables I and II. Certain

additional information is obtainable from these tabulations. In particular, Reynolds number and Mach number based on the inviscid solution for pressure, temperature, and velocity at the cone surface are included. These parameters could serve as independent variables for the data presented, and may have some advantage in certain theoretical comparisons, since boundary-layer theory utilizes these variables. Free-stream parameters were used in their place for the sake of simplicity.

3.0 ACCURACY

The magnitude of error in the force measurement was possibly one to two milligrams for the one-inch model and two to three milligrams for the two-inch model. This estimate is based on observed hysteresis during calibration and repeatability during test and calibration. Such errors amount to a maximum error of slightly over one per cent of the measured force for the Mach 2 tests and slightly under one per cent for the Mach 4 tests.

Hystersis amounted to about 0.2 per cent of the maximum load. It was observable in approximately equal measure in calibration of the Wiancko unit by itself and in calibration of the balance as a whole. It seems likely, therefore, that hystersis effects in the model support were negligible. This conclusion is well supported by a study of the possible magnitude of hystersis due to the support.

Additional scatter stems from correction of the force readings for temperature, which is complicated by the inevitable thermal transients associated with control of the housing temperature. The magnitude of the temperature correction was in general less than five milligrams. Since the temperature coefficient could be determined accurately to five per cent or better, the only appreciable error in correcting for temperature was in the temperature determination itself. If the balance and housing temperature are uniform, precise determination of temperature is possible by the measurement of the Wiancko coil resistance. During heating or cooling, however, the Wiancko coil temperature lags the armature temperature, and is therefore not a reliable measure of the temperature influencing the

Wiancko gaps. To diminish the error from this cause, care was taken to make measurements only during near-equilibrium thermal conditions.

Force errors due to the model support structure were probably negligible. Measurement of restoring force and calculation of thermal effect supports this; however, testing experience does raise doubts. In the tests of the two-inch model no support influence was detectable, but in the tests of the one-inch model an appreciable temperature effect due to the support was present. This defect was presumably caused by minor misalignment of the support members. Its effect was only to increase the thermal zero shift, not to alter the gradient, so that it was taken care of by the normal technique of temperature correction, and no correction of the Wiancko gradient was required. Its presence, however, increased the possibility of scatter due to temperature corrections.

Unfortunately, hidden sources of error are present in the apparatus that conceivably could overwhelm the observed scatter and hystersis. One grave possibility is undetected error due to calibration changes during test. The Wiancko unit is capable of appreciable zero shifts if subjected to moderate mechanical or thermal shocks. Shifts of the order of 10 to 20 miligrams are quite possible from such cause. It seems likely, however, that any shocks capable of producing such changes would occur during starting and during temperature adjustment at the first (and always the highest) flow rate. Since the zero readings were always taken at the conclusion of the run, and since the schedule of flow rate was such that the forces progressively decreased, the liklihood of appreciable zero shifts between successive flow rates and between flow and no-flow conditions does not seem strong.

Also present to raise doubts about the validity of the force measurements is the possible influence of temperature gradients within the balance. The design of the Wiancko unit is such that slight differences in temperature of the legs supporting the armature produce serious changes in reading. The housing was designed to minimize such temperature gradients; however, it must be recognized as a possibility that the distribution of temperature in the balance may have been dif-

ferent during test and during calibration.

A pessimistic view of possible hidden errors in the force determination does not seem justified, in view of the apparent consistency of the test results. The original estimate of about one per cent or better accuracy in the force measurements seems the most reasonable. It should perhaps be noted, however, that attainment of such accuracy with the present equipment requires care and patience.

The primary source of error is almost certainly the determination of free-stream static pressure, which could not be measured by direct means. In the Mach 4 nozzle, the nozzle wall pressure was considered an approximate measure of the free-stream pressure. Previous experience with this nozzle indicates that such an assumption should be reliable within one to two per cent or better. The nozzle has been found to have shock-free expansion, the variation in impact pressure throughout the test cone being no more than one per cent (Ref. 3). In this nozzle, therefore, the free-stream pressure determination, though an important source, is not a large source of error.

The Mach 2 nozzle is a different story. Impact-pressure measurements of the test region reveal appreciable pressure gradients and evidence of imperfect expansion (Ref. 4). Since evaluation of the free-stream properties is at present not possible without the assumption of isentropic expansion, a sure picture of the nature of the test region is not obtainable. Axial pressure variation calculated from stagnation and impact pressures in Ref. 4 amounts to six per cent at the highest flow rate and 16 per cent at the lowest, over the region between the cone tip location and a point two inches downstream. Corresponding Mach-number variation amounts to two per cent at the highest flow and five per cent at the lowest. Because of these apparent nonuniformities, accurate specification of free-stream properties for the present tests would not be possible even with direct measurement.

The indirect determination of free-stream pressure from wall-pressure measurements is possible in the Mach 2 nozzle, but the wall pressure is not so reliable a guide as in the Mach 4 nozzle. Because

of wall shocks, the wall pressure is normally two to ten per cent above the (presumed) free-stream pressure. The ratio of wall pressure to free-stream pressure is predictable as a function of flow rate, so that the wall pressure measurement could serve to establish the free-stream pressure. It was decided, however, that prediction of free-stream Mach number had a better chance of accuracy than prediction of this pressure ratio. The free-stream Mach number, like the wall-to-stream pressure ratio, is available from the nozzle calibration of Ref. 4. It is estimated that the static pressure resulting from this assumption is within about five per cent of the appropriate free-stream value.

The errors in determination of pressures other than the static pressure are not significant. Stagnation pressure was measured directly to an accuracy of better than one-half per cent in the Mach 2 nozzle and better than 0.2 per cent in the Mach 4 nozzle. Cone-pressure measurement was even more precise. Possible error in temperature measurement is also unimportant, but might be as large as one-half per cent.

Based on the foregoing considerations of force, pressure, and temperature accuracy, an estimate of possible error in drag coefficient and Reynolds number can be obtained. The preceding discussion suggests the use of the following figures as representative of the accuracy of data from the Mach 2 nozzle: force, one per cent; static pressure, five per cent; stagnation pressure, one-half per cent; cone pressure, one-half per cent; stagnation temperature, one-half per cent. For the Mach 4 nozzle the same figures may be considered to apply except for the static and stagnation pressures, for which figures of two per cent and 0.2 per cent, respectively, will be considered to obtain. Based on the assumption of isentropic expansion the corresponding accuracy in Mach number and dynamic pressure is two per cent for each in the Mach 2 nozzle, and one-half per cent and one and one-half per cent, respectively, in the Mach 4 nozzle. The associated errors in drag coefficient amount to five per cent for the Mach 2 nozzle and two and one-half per cent for the Mach 4 nozzle, with corresponding Reynolds number error of two and one-half and one and one-half per cent. These figures are in general

indicative of the accuracy at the lowest Reynolds numbers; however, most of the error can be traced to static pressure error, which will exert comparable influence at high Reynolds number.

Besides the possible errors in measurement, there are possible errors in simulation of the desired flow. The tests were intended to simulate adiabatic flow over an infinite cone in an infinite uniform flow field. With the exception of the uniformity of flow, which has already been discussed, it is probable that all of these requirements have been satisfactorily met. Some departure from adiabatic flow was present, but probably not serious. The stagnation temperature for the tests was room temperature, so that the recovery temperature of the air adjacent to the model surface was somewhat below the temperature of the surroundings. The possible heat transfer, however, even with the model surface at room temperature, was small: calculation reveals a possible error from this source of around one per cent. It is reasonable, therefore, to interpret the data as valid for an adiabatic wall.

The finite extent of the cone and the flow field were evidently not serious flaws. Of course there was no real desire to simulate an infinite cone nor an infinite flow field. More properly stated it was desired simply that the limits of the cone and the flow field be far enough away to be uninfluencial. The requirements appear to have been met. The change in ratio of model length to total length of the conical surface does not appear to have influenced the flow over the model appreciably: no "shoulder effect" is detectable in the data. Also, analysis of possible boundary interference indicates that the extent of the flow field is probably adequate; and, again, the data display none of the symptoms of imperfection.

From this analysis of accuracy, the major defects of the tests become clear. Improvement in accuracy over the range of the present tests requires use of a better Mach 2 nozzle, and more precise determination of free-stream properties. In addition to these requirements, extension to low Reynolds number requires improvement of force measurement. Reduction of model length by two, for example will reduce the measured force by about three, and begin to make force errors significant.

Failure of the first-order boundary-layer terms to predict the proper drag, encourages contemplation of possible second-order effects. These effects may arise from three sources: interaction between boundary layer and the adjacent stream, rarefaction, or boundary-layer curvature. These influences all become important in a compressible flow if the Reynolds number is sufficiently decreased.

Apparently the first of these to gain prominance in a supersonic flow is the interaction. A part of the drag due to interactions is already included in the present boundary-layer calculation, since interaction gives rise to a first-order pressure-drag term. A second-order pressure-drag term as well as a second-order shear term, are also obtainable by further analysis of the interaction. Of these, the shear term is almost certainly the more significant. Its value could be obtained by recalculation of the boundary layer to account for the induced pressure gradient and change in pressure level at the seam of the boundary-layer. An evaluation of this term has been made for a flat plate by Maslen (Ref. 7) and, for hypersonic flow, by Lees and Probstein (Ref. 8). It is probable that much of the deviation between the present tests and the first-order boundary-layer theory at the higher Reynolds numbers can be accounted for in the analogous second-order shear term for the cone.

Rarefaction will also introduce higher-order terms, but probably nothing much of second order. This presumption is based on the flat-plate analyses of Maslen (Ref. 7) and Lin and Schaaf (Ref. 9). Maslen considers all rarefaction phenomena within the framework of boundary-layer theory and concludes that, to the second order, rarefaction effects appear only in the boundary conditions (viz. as slip and temperature jump). He further finds the shear unaffected to the second order. Lin and Schaaf (considering only slip) reach the same conclusion. In addition they evaluate a displacement thickness change. Such a change would, for the cone, give rise a second-order pressure-drag term, but second-order pressure drag terms arising from a change in boundary-layer thickness can hardly amount to much, whether from slip or interaction.

Like interaction, boundary-layer curvature may also be an important source of second-order effects. Boundary-layer theory assumes that the boundary-layer is "flat", i.e., that its thickness is small compared to the radius of curvature of the streamlines or the wall. It is not likely that the streamline curvature is sufficient to introduce any large second-order effects; however, the curvature of the cone surface normal to the flow direction can probably not be ignored. Seban and Bond's analysis of axial flow over a cylindrical surface (Ref. 10) suggests that a second-order shear term of appreciable magnitude may be present from this cause.

Analysis of these various influences has not been extended to the cone. Although flat-plate boundary-layer solutions can be transformed by the Mangler transformation, the transformation does not yield the corresponding physical solution for the cone if interaction or slip is present. This shortcoming of the Mangler transformation is demonstrated in Appendix E. The effect of boundary-layer curvature is also unknown for the cone. The Mangler transformation, being subject to the usual boundary-layer restrictions, cannot be expected to provide any clues. Speculation about the nature of flow over a cone is therefore difficult with only flat-plate analysis as a guide.

Besides looming large, the task of evaluating the second-order corrections to shear and pressure may prove unprofitable. The deviations between theory and experiment do not appear susceptible to so easy an explanation. Close analysis of the differences between theoretical and experimental points suggest a second-order deviation only at the highest Reynolds numbers. Uncertainties in the data supply a restraint to drawing positive inferences from the results; however, there are unmistakable trends in the nature of the deviations as the Reynolds number decreases (see Figure 7). At the highest Reynolds numbers the deviations are proportional to R_1^{-1}, but as the Reynolds number decreases the exponent of R_1 increases continuously to a value of $-\frac{1}{2}$ or more. The conclusion suggested by these observations is that not only second-order, but third- and higher-order influences are rapidly coming into prominance at

these low Reynolds numbers.

The present idea of ordering terms may therefore prove unsatisfactory. Because of the asymptotic nature of the boundary-layer approach, it inevitably breaks down toward the cone tip. If the tip region is not a small fraction of the flow, the use of the ordinary boundary-layer solution as a starting point is inappropriate: such an approach has no chance of describing the tip flow. Prominence of the tip flow in the over-all drag picture appears to be indicated by the present tests.

The hypersonic analysis of Lees (Ref. 11) demonstrates the changes in viewpoint that may be required. From analysis of two-dimensional flow he finds that in regions of "strong interaction" between the boundary layer and the exterior flow, the "first-order" shear is not expressed by the usual boundary-layer solution. Instead he finds the first approximation to the shear to be proportional to $R^{-\frac{3}{4}}$. This analysis has not been extended to the cone, so that estimates of the strength of interaction and the nature of the possible shear terms, are not available. Furthermore, in the present regime of flow it is likely that an analysis of the strong interaction region should also include slip, which is neglected in the hypersonic analysis. However, the chances appear good that the presence of some sort of strong interaction between the boundary flow and the exterior flow at the tip is having appreciable influence, and that mere refinements to boundary-layer results will not be adequate to explain the observed discrepancies.

The present results, then, provide possible indications of the nature of the cone viscous layer. Some support for the present interpretations is also provided by the flat-plate data of Sherman (Ref. 12), who finds comparable deviations from bounday-layer theory. Further drag investigations at lower Reynolds number and over a more continuous range of Mach number are greatly needed to support the development of satisfactory theory, but even the present results are suggestive of the complexity of the problem.

5.0 CONCLUSIONS

(1) The drag coefficient curves are probably accurate to two to three per cent or better at Mach 4 and perhaps five per cent at Mach 2. Major source of error is in determination of free-stream conditions. Better control or evaluation of flow conditions is a prerequisite for better results.

(2) Compared to boundary-layer theory, the results show similar trends and comparable Mach-number dependence, but greater drag. Experimental results for viscous drag are 10 to 30 per cent above predictions based on first-order boundary-layer analysis of shear and pressure distribution. The difference between theory and experiment does not appear to be explainable in terms of second-order deviations from the boundary-layer theory.

(3) Force measurements appear to have been sufficiently accurate for the purposes of the present investigation, but accuracy will become marginal at Reynolds numbers appreciably below those investigated. Temperature sensitivity and susceptibility to calibration change make the balance difficult to use. Improvements in ruggedness and better control of or compensation for temperature are indicated.

(4) Pressure within the housing does not appear to provide a precise measure of cone surface pressure. This defect does not influence the total drag detectably. It does, however, make separation of pressure and shear drag impossible without supplementary cone pressure data.

APPENDIX A

DESCRIPTION OF APPARATUS

A1.0 MODELS AND HOUSING

The two cones were machined of dural. The configuration of the one-inch cone is shown in Figure 3. The two-inch cone was similar; however, the lip was 0.030 inches thick, whereas the one-inch cone was tapered to a 0.005 inch lip to reduce the influence of any pressure disturbance at the gap. The continuation of the conical configuration by the housing gives an over-all cone length of 3.70 inches.

The housing was so designed that internal parts of the balance would be almost completely surrounded by a relatively thick wall of dural that would attain a fairly uniform temperature despite variations in surface heat-transfer rates over the model. The housing is supported by a strut having a diamond cross-section with a 15° half-angle leading edge and a thickness of about half an inch. The strut carries a pressure line from the interior of the housing and also serves to support the external electrical leads.

To provide control of the temperature within the housing, nichrome strip was closely spaced along the cylindrical portion of the housing and covered with a layer of asbestos. A layer of drafting tape insulates the strip from the housing. Similar tape was used to secure the asbestos. The heater has a resistance of about 5 ohms, and was supplied with 0.3 to 1.3 amperes, depending on heating requirements.

The gap between the model and housing was designed to be 0.010 inches for the two-inch model and 0.005 inches for the one-inch model. These values were not met with precision in the final assembly, the gaps being perhaps 10 to 20 per cent oversize. Precise adjustment of the model position was difficult. Alignment of the model was adjusted visually, and minor deviations (of the order of 0.001 to 0.002 inches) were detectable in the final assembly.

A2.0 MODEL SUPPORT

The models are supported by a sting (Figure 3, Part 29) that attaches to a yoke (Part 27) surrounding the Wiancko unit. The yoke is supported at two points by 0.005-inch lateral wires. The wires are strung between vertical members at the bottom of which are similar wires that attach to fixed points directly below the points of attachment of the yoke. Tension in the wires is controlled by differential-pitch turnbuckles (Part 22) running between the vertical members.

Support of the model from below gives rise to a negative restoring force that counteracts the small positive restoring force of the wires. Additional counteraction is obtained by adding weights (Part 59) to the tops of vertical members. By adjustment of the magnitude and position of the counterweights, the restoring force of the wires can be completely compensated, so that the supporting structure exerts no restraint on the axial motion of the model and yoke. In practice the restoring force of the support was reduced to $\pm$ 0.1 per cent or less of the Wiancko restoring force.

A3.0 WIANCKO UNIT

A hair (Figure 3, Part 1) connects the yoke to the armature of the Wiancko unit. The armature is flexibly supported about its center, so that application of force at the upper end widens the upper gap and narrows the lower, thus changing the relative reluctance of the two magnetic circuits. Deflection of the end of the armature amounts to about 10^{-6} inches per milligram. Three leads from the Wiancko unit are carried out of the housing through waxed seals at the rear (Part 7).

The Wiancko unit was operated with gaps between the armature and the pole pieces of about 0.020 inches. When supplied with 3.2-kilocycle, 20-volt power it gave a midpoint voltage swing of about 0.12 millivolts per milligram.

The unit was originally supplied by the Wiancko Engineering Company of Pasadena. The present unit includes minor modifi-

cations in gap size, casing, and method of force application.

A4.0 MEASURING CIRCUIT

Power supply for the measuring circuit is a Hewlitt-Packard oscillator (Type 200 AB). Force measurement utilizes the 200-ohm helipot which has a guaranteed linearity of 0.1 per cent. The decade voltage divider permits shifting of the helipot zero as the load range changes. The decade resistor and zeroing helipot, which provide additional range and zero control, were maintained at fixed values of 3000 and 80 ohms, respectively, during all testing.

The d-c bridge circuit shown was used to measure the Wiancko resistance, which serves as an indication of the temperature within the model housing. Measurement of resistance change was accurate to about 0.01 ohms, or better than 0.02 per cent. In terms of temperature this amounts to better than 0.1°F accuracy. The circuit was so designed that the dissipation in the Wiancko unit during resistance measurement was about the same as during normal operation in the force-measuring circuit, thereby minimizing the thermal transient accompanying switching.

All fixed resistors in the circuits were wound from manganin, baked, and vacuum impregnated.

A5.0 WIND TUNNEL

The tests were performed in the continuous-flow open-jet wind tunnel described in Ref. 13. The basis for design of the Mach 2 nozzle (No. 6) is described in Ref. 14, and the performance in Ref. 4; the design and performance of the Mach 4 nozzle (No. 8) are described in Ref. 3.

The tunnel is instrumented with a precision butyl-phthalate U-tube manometer, described in Ref. 15, and a precision mercury McLeod gage, described in Ref. 16, for pressure measurement. Tunnel pressure level is controllable by throttling the flow from the test chamber into the ejectors that drive the tunnel. Flow rate into the tunnel is measured by a rotameter.

APPENDIX B

TEST PROCEDURE

B1.0 TUNNEL OPERATION

All testing was performed with the tip of the cone centered in the nozzle and one inch upstream from the exit plane (see Figure 1). This selection was based on exploratory axial traverses of the two-inch model.

Prior to each run the balance housing and connecting pressure leads were leak tested with a mass spectrograph. All tests reported are for operation without detectable leaks.

Standard tunnel conditions were secured by setting the ejector valve to give equality of the chamber pressure and wall pressure at the exit of the nozzle: i.e., a "balanced" jet.

Stagnation-chamber pressure, nozzle-wall pressure, test-chamber pressure and cone pressure were measured with the McLeod gage when possible, and with the manometer. Stagnation-chamber temperature was measured with an iron-constantan thermocouple.

The temperature within the model housing was maintained approximately constant at a standard value of about 100°F by manual control of the heating current. Drag readings and Wiancko resistance readings were taken three to five or more times at each flow condition. Zero readings were taken at the conclusion of the run before the tunnel was brought up to atmospheric pressure.

B2.0 CALIBRATION

After each run the plug (Figure 3, Part 57) was removed from the bottom of the housing and a calibration performed over the range of readings encountered during the run. Two such calibrations were made: one at or near the standard temperature and one at ambient temperature. Normally the Wiancko resistance changed about five ohms between the calibrations. These calibrations were used to correct the drag readings to the standard temperature.

Upon completion of tests of one model, the Wiancko unit was calibrated directly. This was accomplished by partial disassembly of the balance so that weights could be hung directly from the hair (Part 1). The calibration was conducted in the tunnel with the housing swung into a vertical position and the Wiancko unit returned to approximately its original location inside. Again calibrations were made at two temperatures so that corrections could be made to the standard temperature.

Class S analytical balance weights were used in the calibrations. Subsequent calibration of the weights revealed a maximum error, for the weights used, of 0.03 mg.

APPENDIX C

REDUCTION OF DATA

C1.0 CALIBRATION DATA

Based on calibrations at two temperatures, the temperature response of the Wiancko unit was plotted as a function of potentiometer reading, and from this all calibration points were corrected to the standard temperature. Deviations of the corrected calibration from a basic straight-line calibration were then plotted. These deviations amounted to several milligrams, and followed a consistent pattern as a function of potentiometer reading.

C2.0 TEST DATA

Force readings were corrected to the standard temperature by use of the secondary balance calibration, and converted to milligrams by use of the Wiancko calibration. In this conversion, correction was made for the non-linearities in the Wiancko calibration.

In the Mach 4 nozzle free-stream conditions were based on the measured stagnation chanber temperature and pressure and the nozzle wall pressure, the latter being assumed equal to the free-stream static pressure. The nozzle flow was assumed isentropic with $\gamma = 1.40$.

The isentropic flow assumption was also made for the Mach 2 nozzle; however, wall pressure measurements were ignored in determining free-stream conditions. Instead, Mach numbers were assumed equal to those measured at the cone tip location (one inch upstream from the exit plane) in independent nozzle calibrations at the same flow rates (Ref. 3).

Reynolds-number evaluation was based on viscosity obtained from Sutherland's equation for air, as tabulated in Ref. 17. The thermodynamic properties were based on the perfect-gas law for air.

Ideal cone-surface conditions were obtained by use of plots made from the Kopal tables (Ref. 18).

C3.0 CORRECTION FOR MACH NUMBER

Correction of the drag-coefficient data to constant values of Mach number of 2 and 4 utilized the comparison between test and theory discussed in Section 4.0. The theoretical changes in the value of viscous drag coefficient $C_D - C_{Di}$ between test conditions and the standard Mach numbers of 2 and 4 (as determined from the equations of Appendix D) were added to the test values of $C_D - C_{Di}$ to give the corrected viscous drag coefficients. Corrected values of total drag coefficient C_D were then obtainable by addition of the inviscid drag coefficients corresponding to Mach numbers 2 and 4. For convenience, correction was made to a constant stagnation temperature of T_o = 530°R as well as to constant values of Mach number.

APPENDIX D

THEORETICAL DRAG

D1.0 SHEAR DRAG

As a first approximation the skin friction can be evaluated by transforming the boundary layer on a flat plate by the Mangler transformation (Ref. 19, see also Appendix E). For a flat plate with no pressure gradient, slip, nor heat transfer, Young (Ref. 20) gives for the integrated shear coefficient,

$$\bar{C}_f' = \frac{1.328}{\sqrt{R_x}}\left[1 + 0.365(\gamma-1)M^2\sigma^{\frac{1}{2}}\right]^{\frac{\omega-1}{2}} \qquad \text{(D-1)}$$

For such a boundary layer the transformation to a cone is simply

$$C_f' = \frac{2}{3}\sqrt{3}\,\bar{C}_f' = \frac{1.533}{\sqrt{R_{ci}}}\left[1 + 0.365(\gamma-1)M_{ci}^2\sigma^{\frac{1}{2}}\right]^{\frac{\omega-1}{2}} \qquad \text{(D-2)}$$

if the flow at the seam of the boundary layer is presumed to approximate the inviscid solution. Expressed as a shear drag coefficient Eq. D-2 becomes

$$C_{D_f}' = \frac{1.533}{\sqrt{R_1}}\left[1 + 0.365(\gamma-1)M_{ci}^2\sigma^{\frac{1}{2}}\right]^{\frac{\omega-1}{2}}\left(\frac{q_{ci}}{q_1}\right)\left(\frac{R_1}{R_{ci}}\right)^{\frac{1}{2}}\cot\alpha \qquad \text{(D-3)}$$

For $\gamma = 1.40$, $\sigma = 0.723$, $\omega = 0.785$ and $\alpha = 15°$, Eq. D-3 becomes

$$C_{D_f}' = \frac{5.723}{\sqrt{R_1}}\left[1 + 0.1241\,M_{ci}^2\right]^{-0.1075}\left(\frac{q_{ci}}{q_1}\right)\left(\frac{R_1}{R_{ci}}\right)^{\frac{1}{2}} \qquad \text{(D-4)}$$

D2.0 PRESSURE DRAG

The pressure distribution can be approximated by evaluating the inviscid pressure on a cone tangent to the boundary layer (the local tangent-cone approximation, Ref. 5). Such a cone would have a half-angle of

$$\beta = \alpha + \theta = \alpha + \tan^{-1}\left(\frac{d\delta^*}{dx}\right) \doteq \alpha + \frac{d\delta^*}{dx} \qquad \text{(D-5)}$$

(see Figure 10). The displacement thickness δ^* may be approximated by Howarth's flat-plate boundary layer (Ref. 21), which corresponds to ω and σ of unity. Use of the less-exact Howarth solution is justifiable for the pressure drag, since the effect of the boundary layer on pressure is small compared to its effect on shear. The Howarth displacement thickness transforms by the Mangler transformation to

$$\frac{\delta^*}{x} = 2\frac{d\delta^*}{dx} = \frac{1}{\sqrt{R_x}}\left(1 + 0.277 M_{ci}^2\right) \tag{D-6}$$

so that

$$\beta = \alpha + \frac{1}{2\sqrt{R_x}}\left(1 + 0.277 M_{ci}^2\right) \tag{D-7}$$

The relationship between β and the pressure may be satisfactorily approximated, for present purposes, by a tangent to the inviscid solution for cone pressure as a function of cone angle. This approximation evaluates the first-order correction; closer approximation of the relationship gives terms of higher order in $R_1^{-\frac{1}{2}}$. With this approximation

$$\frac{p_x - p_{ci}}{p_1} = (\beta - \alpha) f(\alpha, M_1) \tag{D-8}$$

where

$$f(\beta, M_1) = \frac{1}{p_1}\left(\frac{\partial p_x}{\partial \beta}\right)_{M_1} \tag{D-9}$$

The function f is the slope of the tangents to constant M_1 lines in the p_x/p_1 vs. β plane. From Eqs. D-7 and D-8

$$p_x = p_{ci} + p_1 \frac{f}{2\sqrt{R_x}}\left(1 + 0.277 M_{ci}^2\right) \tag{D-10}$$

The pressure drag is therefore

$$\begin{aligned} D_p &= 2\pi \sin^2\alpha \int_0^L p_x x\,dx - p_1 A_f \\ &= A_f\left[p_{ci} - p_1 + \frac{2}{3} p_1 \frac{f}{\sqrt{R_{ci}}}\left(1 + 0.277 M_{ci}^2\right)\right] \end{aligned} \tag{D-11}$$

with the corresponding drag coefficient

$$C'_{D_p} = C_{Di} + \frac{4}{3\gamma}\frac{1}{\sqrt{R_1}}\frac{f}{M_1^2}\left(1 + 0.277 M_{ci}^2\right)\left(\frac{R_1}{R_{ci}}\right)^{\frac{1}{2}} \qquad \text{(D-12)}$$

where C_{Di} is the inviscid drag coefficient.

APPENDIX E

THE MANGLER TRANSFORMATION AND ITS LIMITATIONS

The Mangler transformation (Ref. 19) provides a technique for transforming compressible two-dimensional boundary-layer solutions to rotationally symmetric bodies. If x and y are coordinates along the boundary layer and normal to it, respectively, and u and v are the corresponding velocities, the boundary-layer equations for a rotationally symmetric body are, for a perfect gas with constant specific heats,

$$\rho u \frac{\partial u}{\partial x} + \rho v \frac{\partial u}{\partial y} = - \frac{\partial p}{\partial x} + \frac{\partial}{\partial y}\left(\mu \frac{\partial u}{\partial y}\right) \tag{E-1}$$

$$\frac{\partial}{\partial x}(\rho r u) + \frac{\partial}{\partial y}(\rho r v) = 0 \tag{E-2}$$

$$\rho c_p u \frac{\partial T}{\partial x} + \rho c_p v \frac{\partial T}{\partial y} = u \frac{\partial p}{\partial x} + \frac{\partial}{\partial y}\left(k \frac{\partial T}{\partial y}\right) + \mu \left(\frac{\partial u}{\partial y}\right)^2 \tag{E-3}$$

where r is the radius of the body, a function of x. These equations are based on the same approximations as two-dimensional boundary-layer theory, except that the requirement that the boundary-layer thickness be small relative to the radius of curvature of the wall is generalized to include both radii of curvature.

The Mangler transformation transforms these coordinates by the following relations:

$$\bar{x} = \int_0^x \left(\frac{r}{l}\right)^2 dx \tag{E-4}$$

$$\bar{y} = \frac{r}{l} y \tag{E-5}$$

$$\frac{\partial}{\partial x} = \frac{r^2}{l^2} \frac{\partial}{\partial \bar{x}} + \frac{y}{r} \frac{dr}{dx} \frac{\partial}{\partial \bar{y}} \tag{E-6}$$

$$\frac{\partial}{\partial y} = \frac{r}{l} \frac{\partial}{\partial \bar{y}} \tag{E-7}$$

The dependent variables are similarly transformed; however, all but V go over unchanged:

$$u(x,y) = \bar{u}(\bar{x},\bar{y}) \tag{E-8}$$

$$v(x,y) = \frac{r}{\ell}\bar{v}(\bar{x},\bar{y}) - \frac{y}{r}\frac{dr}{dx}\bar{u}(\bar{x},\bar{y}) \tag{E-9}$$

$$p(x) = \bar{p}(\bar{x}) \tag{E-10}$$

$$T(x,y) = \bar{T}(\bar{x},\bar{y}) \tag{E-11}$$

$$\mu(x,y) = \bar{\mu}(\bar{x},\bar{y}) \tag{E-12}$$

$$\rho(x,y) = \bar{\rho}(\bar{x},\bar{y}) \tag{E-13}$$

$$k(x,y) = \bar{k}(\bar{x},\bar{y}) \tag{E-14}$$

With these transformation equations E-1, E-2 and E-3 become

$$\bar{\rho}\bar{u}\frac{\partial\bar{u}}{\partial\bar{x}} + \bar{\rho}\bar{v}\frac{\partial\bar{u}}{\partial\bar{y}} = -\frac{\partial\bar{p}}{\partial\bar{x}} + \frac{\partial}{\partial\bar{y}}\left(\bar{\mu}\frac{\partial\bar{u}}{\partial\bar{y}}\right) \tag{E-15}$$

$$\frac{\partial}{\partial\bar{x}}(\bar{\rho}\bar{u}) + \frac{\partial}{\partial\bar{y}}(\bar{\rho}\bar{v}) = 0 \tag{E-16}$$

$$\bar{\rho}c_p\bar{u}\frac{\partial\bar{T}}{\partial\bar{x}} + \bar{\rho}c_p\bar{v}\frac{\partial\bar{T}}{\partial\bar{y}} = \bar{u}\frac{\partial\bar{p}}{\partial\bar{x}} + \frac{\partial}{\partial\bar{y}}\left(\bar{k}\frac{\partial\bar{T}}{\partial\bar{y}}\right) + \bar{\mu}\left(\frac{\partial\bar{u}}{\partial\bar{y}}\right)^2 \tag{E-17}$$

These equations are identical to the boundary-layer equations for two-dimensional flow. In the transformation equations ℓ is an arbitrary length. Associated with these transformations, one can also write for the boundary-layer thickness and wall shear

$$\delta^*(x) = \frac{\ell}{r}\,\bar{\delta}^*(\bar{x}) \tag{E-18}$$

$$\tau_x(x) = \frac{r}{\ell}\,\bar{\tau}_{\bar{x}}(\bar{x}) \tag{E-19}$$

The latter equation is strictly valid only for zero slip or alternatively for zero wall curvature in the flow direction. If, however, slip and wall curvature are both present, it is merely necessary that the mean free path be small compared to radius of curvature. Since a slip boundary-layer solution is limited to mean free paths small compared to the boundary-layer thickness, Eq. E-19 is clearly a safe approximation even with slip.

For the cone

$$r = x \sin\alpha \tag{E-20}$$

so that the transformation is simplified to the extent that dr/dx is a constant$(\sin\alpha)$, and, more important, Eq. E-4 can be integrated to give

$$\bar{x} = \frac{1}{3}\,\frac{x^3}{\ell^2}\,\sin^2\alpha \tag{E-21}$$

Thus the flat-plate solutions for shear and displacement thickness (with zero slip and zero pressure gradient),

$$\bar{\tau}_{\bar{x}} = \frac{C_1}{\sqrt{\bar{x}}} \tag{E-22}$$

$$\bar{\delta}^* = C_2\sqrt{\bar{x}} \tag{E-23}$$

transform, respectively, to

$$\frac{\ell}{x\sin\alpha}\,\tau_x = \frac{C_1}{\sqrt{x}}\,\frac{\sqrt{3}\,\ell}{x\sin\alpha} \quad ; \quad \tau_x = \sqrt{3}\,\frac{C_1}{\sqrt{x}} \tag{E-24}$$

$$\frac{x\sin\alpha}{\ell}\,\delta^* = C_2\sqrt{x}\,\frac{x\sin\alpha}{\sqrt{3}\,\ell} \quad ; \quad \delta^* = \frac{1}{\sqrt{3}}\,C_2\sqrt{x} \tag{E-25}$$

The boundary conditions transform unchanged, making these equations a valid statement of the boundary-layer solution for the cone (again, with zero slip and zero pressure gradient).

Unfortunately, the physical correspondence of flat-plate and cone solutions is destroyed if pressure gradient is introduced. The transformation does not permit control of the pressure boundary condition, which in general suffers distortion in the transformation. It is immediately evident, therefore, that if one transforms a flat-plate solution with a self-induced pressure gradient, the chance is remote that the transformed solution will correspond to the cone solution with a self-induced pressure gradient. For all practical purposes the flat-plate with zero pressure gradient is apparently the only flat-plate solution that transforms into the corresponding physical solution for the cone.

A similar and more easily demonstrable complication arises in the transformation of slip solutions. If the two-dimensional solution has the simple slip boundary condition

$$\bar{u}_{\bar{x}} = \epsilon \bar{\tau}_{\bar{x}} \quad ; \quad \bar{v}_{\bar{x}} = 0 \tag{E-26}$$

where ϵ is presumed a constant (equal approximately to the ratio of mean free path to viscosity), the transformed boundary condition for the rotationally symmetric body is, from Eqs. E-8, E-9 and E-19,

$$u_x = \epsilon \frac{l}{r} \tau_x \quad ; \quad v_x = 0 \tag{E-27}$$

The constant slip coefficient has thus transformed to a slip coefficient varying inversely with body radius.

It seems clear, then, that the Mangler transformation is of limited utility in making flat-plate solutions available to the cone, unless the boundary conditions of the flat-plate soultion are so general that the transformed boundary conditions can be adjusted to match the physical requirement of the cone flow. Analysis of the effect of slip or self-induced pressure gradients cannot be borrowed from flat-plate investigations; direct investigation of the cone problem is necessary.

REFERENCES

1. T. S. Lin, S. A. Schaaf, F. S. Sherman — "Boundary Layer Effect on the Surface Pressure of an Infinite Cone in Supersonic Flow", Univ. of Calif. Eng. Projects Report HE-150-80, March 1951. (The major portion of this report is reproduced as Appendix A of Ref. 6)

2. R. M. Drake, G. J. Maslach — "Heat Transfer from Right Circular Cones to a Rarefied Gas Flow in Supersonic Flow", Univ. of Calif. Eng. Projects Report HE-150-91, April 1952.

3. J. M. Owen, F. S. Sherman — "Design and Testing of a Mach 4 Axially Symmetric Nozzle for Rarefied Gas Flows", Univ. of Calif. Eng. Projects Report HE-150-104, July 1952.

4. — "Calibration and Evaluation of No. 6 Nozzle", (N.B. 309), Univ. of Calif. Low Pressures Project (unpublished).

5. D. M. Ehret — "Accuracy of Approximate Methods for Predicting Pressures on Pointed Non-lifting Bodies of Revolution in Supersonic Flow", N.A.C.A. Tech. Note 2764, August 1952.

6. L. Talbot — "Viscosity Corrections to Cone Probes in Rarefied Supersonic Flow at a Nominal Mach Number of 4", Univ. of Calif. Eng. Projects Report HE-150-113.

7. S. A. Maslen — "Second Approximation to Laminar Compressible Boundary Layer on Flat Plate in Slip Flow", N.A.C.A. Tech. Note 2818, November 1952.

8. L. Lees, R. F. Probstein — "Hypersonic Viscous Flow over a Flat Plate", Princeton Univ. Aero. Eng. Lab. Report No. 195, April 1952.

9. T. C. Lin, S. A. Schaaf — "The Effect of Slip on Flow Near a Stagnation Point and in a Boundary Layer", Univ. of Calif. Eng. Projects Report HE-150-76, October 1950.

10. R. A. Seban, R. Bond — "Skin Friction and Heat-Transfer Characteristics of a Laminar Boundary Layer on a Cylinder in Axial Incompressible Flow", Journal Aero. Sci. Vol. 18, No. 10, October 1951.

11. L. Lees — "On the Boundary Layer Equations in Hypersonic Flow and Their Approximate Solutions", Princeton Univ. Aero. Eng. Lab. Report No. 212, September 1952.

12. F. S. Sherman — "Skin Friction in Supersonic Low Density Gas Flow (Part 2)", Univ. of Calif. Eng. Projects Report HE-150-81, March 1951.

13. E. D. Kane — "Drag Forces on Spheres in Low Density Supersonic Gas Flow", Jour. Aero. Sci. Vol. 18, No. 4, pp 259-270, April 1951, also Univ. of Calif. Eng. Projects Report HE-150-64, February 1950.

14. D. E. Emerson, S. A. Schaaf — "Performance of a Supersonic Nozzle in the Rarefied Gas Dynamics Regime", Univ. of Calif. Eng. Projects Report HE-150-72, August 1950.

15. G. J. Maslach — "A Precision Manometer for Low Pressures", Univ. of Calif. Eng. Projects Report HE-150-75, October 1950.

16. F. S. Sherman — "New Experiments on Impact Pressure Interpretation in Supersonic and Subsonic Rarefied Airstreams (Appendix C)", Univ. of Calif. Eng. Projects Report HE-150-99, December 1951.

17. — "The NBS-NACA Tables of Thermal Properties of Gases (Table 2.39)", December 1950.

18. Z. Kopal — "Tables of Supersonic Flow Around Cones", M.I.T. Dept. of Elec. Eng., 1947.

19. W. Mangler — "Zusammenhang zwischen ebenen und rotations-symmetrischen Grenzschichten in Kompressiblen Flüssigkeiter", Z.A.M.M., Vol. 28, 1948.

20. A. D. Young — "Skin Friction in the Laminar Boundary Layer in Compressible Flow", Report 20, College of Aeronautics, Cranfield, England, 1948.

21. L. Howarth — "Concerning the Effect of Compressibility on Laminar Boundary Layers and Their Separation", Proc. Roy. Soc., Ser. A., No. 1036, Vol. 194, pp 16-42 1948.

TABLE I

TEST DATA

	1	2	3	4	5	6	7
RUN NUMBER	NOZZLE NUMBER	MODEL LENGTH	FLOW RATE	STAGNATION PRESSURE	STAGNATION TEMPERATURE	FREE-STREAM PRESSURE	FREE-STREAM TEMPERATURE
		L		p_o	T_o	p_1	T_1
		inches	lb/hr	microns	°R	microns	°R
413	6	2	30	2021	525.0	189.0	266.8
			24	1614	525.6	153.3	268.3
			18	1220	526.8	121.5	272.5
			12	823	527.1	88.6	278.8
			5.2	368	527.6	49.3	297.0
421	6	1	30	2000	537.5	187.0	273.1
			24	1583	538.2	150.4	274.7
			18	1209	537.5	120.4	278.0
			12	813	536.7	87.5	283.9
			5.2	367	535.0	49.1	301.2
414	8	2	26	23,770	537.3	133.6	122.3
			20	18,033	537.3	109.2	124.9
			14	13,069	535.8	89.2	128.8
			10.3	9,947	535.1	73.5	131.7
			5.2	5,045	535.1	50.8	143.8
422	8	1	26	24,150	538.2	135.6	122.4
			20	18,140	539.6	109.6	125.3
			14	13,290	538.5	88.9	128.8
			10.3	9,912	538.9	72.6	132.3
			5.2	5,093	538.2	50.2	143.8

TABLE I - Continued

TEST DATA

	8	9	10	11	12	13	14
RUN NUMBER	FREE-STREAM MACH NUMBER	FREE-STREAM DYNAMIC PRESSURE	FREE-STREAM REYNOLDS NUMBER	MEASURED FORCE	FORCE COEFFICIENT	CONE PRESSURE	CONE PRESSURE COEFFICIENT
	M_1	q_1	R_1	F	C_F	p_c	C_{pc}
		microns		mg		microns	
413	2.20	640.3	1591	956	0.2022	329.4	0.5144
	2.19	514.7	1274	863	0.2271	271.8	0.5281
	2.16	396.8	975	764	0.2607	215.5	0.5412
	2.11	276.1	673	647	0.3173	157.5	0.5704
	1.97	134.0	320	490	0.4952	83.1	0.6204
421	2.20	633.6	762	316	0.2702	314.1	0.5384
	2.19	504.9	604	291	0.3122	287.6	0.5694
	2.16	393.2	469	265	0.3651	222.0	0.5646
	2.11	272.6	324	228	0.4531	161.0	0.5904
	1.97	133.4	156	165	0.6700	90.2	0.6762
414	4.12	1587	7029	1671	0.1426	385.5	0.2429
	4.06	1262	5468	1493	0.1602	314.8	0.2494
	3.97	986.0	4147	1314	0.1805	251.3	0.2549
	3.91	788.3	3238	1182	0.2031	205.3	0.2604
	3.69	483.6	1829	976	0.2733	131.6	0.2721
422	4.12	1612	3568	539	0.1811	432.6	0.2684
	4.06	1268	2739	498	0.2127	350.8	0.2767
	3.99	989.1	2074	447	0.2448	275.7	0.2787
	3.92	781.2	1595	400	0.2774	223.0	0.2855
	3.70	482.3	908	323	0.3628	145.8	0.3023

TABLE I - Continued

TEST DATA

RUN NUMBER	15 TOTAL DRAG D mg	16 TOTAL DRAG COEFFICIENT C_D	17 INVISCID DRAG COEFFICIENT C_{Di}	18 VISCOUS DRAG COEFFICIENT $C_D - C_{Di}$	19 CONE PRESSURE (INVISCID) p_{ci} microns	20 CONE TEMPERATURE (INVISCID) T_{ci} °R
413	1994	0.4217	0.1948	0.2269	313.7	309.0
	1739	0.4576	0.1951	0.2625	253.7	310.4
	1459	0.4979	0.1961	0.3018	199.3	314.5
	1156	0.5670	0.1982	0.3688	143.3	320.5
	740	0.7479	0.2061	0.5418	76.9	337.4
421	601	0.5138	0.1948	0.3190	310.4	316.2
	545	0.5847	0.1951	0.3893	248.9	317.8
	453	0.6241	0.1961	0.4280	197.5	320.8
	364	0.7233	0.1982	0.5251	141.5	326.3
	241	0.9786	0.2061	0.7725	76.6	342.2
414	3533	0.3015	0.1610	0.1405	389.1	170.2
	3013	0.3233	0.1612	0.1621	312.6	172.7
	2512	0.3450	0.1624	0.1826	249.3	176.5
	2156	0.3704	0.1627	0.2077	201.8	179.4
	1573	0.4405	0.1646	0.2759	130.4	191.3
422	1088	0.3656	0.1609	0.2047	395.0	170.4
	944	0.4033	0.1614	0.2419	314.3	173.4
	792	0.4338	0.1623	0.2715	249.4	176.7
	678	0.4701	0.1626	0.3075	199.6	180.3
	500	0.5616	0.1643	0.3973	129.5	191.5

TABLE I - Continued

TEST DATA

RUN NUMBER	21 CONE MACH NUMBER (INVISCID) M_{ci}	22 CONE DYNAMIC PRESSURE (INVISCID) q_{ci} microns	23 CONE REYNOLDS NUMBER R_{ci}	24 CONE BOUNDARY-LAYER KNUDSEN NUMBER K_{ci}	25 SHEAR-DRAG COEFFICIENT (THEORETICAL) C_{Df}'	26 TANGENT-CONE PRESSURE PARAMETER f
413	1.87	769.9	1830	0.0657	0.1547	4.08
	1.86	616.0	1463	0.0730	0.1723	4.06
	1.84	472.3	1114	0.0827	0.1965	3.97
	1.80	324.1	763	0.0976	0.2346	3.82
	1.68	152.0	356	0.1335	0.3331	3.45
421	1.87	761.8	877	0.0948	0.2235	4.08
	1.86	604.4	694	0.1060	0.2502	4.06
	1.84	468.1	537	0.1191	0.2831	3.97
	1.80	320.0	367	0.1407	0.3382	3.82
	1.68	151.3	174	0.1911	0.4765	3.45
414	3.28	2932	9575	0.0503	0.0986	12.40
	3.24	2301	7417	0.0565	0.1108	12.14
	3.19	1773	5643	0.0636	0.1255	11.72
	3.15	1399	4393	0.0712	0.1406	11.43
	3.00	818.8	2446	0.0908	0.1808	10.35
422	3.28	2979	4856	0.0707	0.1385	12.41
	3.24	2317	3716	0.0798	0.1568	12.15
	3.19	1782	2822	0.0902	0.1778	11.75
	3.15	1389	2159	0.1018	0.2017	11.45
	3.00	818.6	1218	0.1292	0.2567	10.43

TABLE I - Continued

TEST DATA

RUN NUMBER	27 VISCOUS PRESSURE-DRAG COEFFICIENT (THEORETICAL) $C_{Dp}' - C_{Di}$	28 VISCOUS DRAG COEFFICIENT (THEORETICAL) $C_D' - C_{Di}$	29 TOTAL DRAG COEFFICIENT (THEORETICAL) C_D'	30 CONE PRESSURE COEFFICIENT (THEORETICAL) C_{pc}'
413	0.0370	0.1917	0.3865	0.5177
	0.0414	0.2137	0.4088	0.5240
	0.0471	0.2436	0.4397	0.5377
	0.0562	0.2908	0.4890	0.5612
	0.0800	0.4131	0.6192	0.6342
421	0.0535	0.2770	0.4718	0.5300
	0.0600	0.3102	0.5053	0.5380
	0.0678	0.3509	0.5470	0.5532
	0.0810	0.4192	0.6174	0.5799
	0.1144	0.5909	0.7970	0.6600
414	0.0283	0.1269	0.2879	0.2664
	0.0319	0.1427	0.3039	0.2714
	0.0359	0.1614	0.3238	0.2797
	0.0402	0.1808	0.3435	0.2862
	0.0511	0.2319	0.3965	0.3079
422	0.0398	0.1783	0.3392	0.2749
	0.0450	0.2018	0.3632	0.2817
	0.0507	0.2285	0.3908	0.2901
	0.0573	0.2590	0.4216	0.2985
	0.0727	0.3294	0.4937	0.3230

TABLE II

DATA CORRECTED TO MACH NUMBER OF 2 AND 4

RUN NUMBER	1 MODEL LENGTH L inches	2 FREE-STREAM MACH NUMBER M_1	3 FREE-STREAM REYNOLDS NO. R_1	4 STAGNATION TEMPERATURE T_o °R	5 STAGNATION PRESSURE p_o microns	6 FREE-STREAM TEMPERATURE T_1 °R	7 FREE-STREAM PRESSURE p_1 microns
413	2	2	1591	530	1868	294.4	238.7
			1274		1495		191.1
			975		1145		146.3
			673		789		100.9
			320		375		48.0
421	1	2	762	530	1789	294.4	228.6
			604		1419		181.3
			469		1102		140.8
			324		760		97.2
			156		366		46.8
414	2	4	7029	530	21,990	126.2	144.9
			5468		17,100		112.7
			4147		12,970		85.5
			3238		10,130		66.8
			1829		5,721		37.7
422	1	4	3568	530	22,320	126.2	147.1
			2739		17,130		112.9
			2074		12,980		85.5
			1595		9,979		65.8
			908		5,683		37.5

TABLE II - Continued

DATA CORRECTED TO MACH NUMBER OF 2 AND 4

RUN NUMBER	8 FREE-STREAM DYNAMIC PRESSURE q_1 microns	9 CONE TEMPERATURE (INVISCID) T_{ci} °R	10 CONE PRESSURE (INVISCID) p_{ci} microns	11 CONE MACH NUMBER (INVISCID) M_{ci}	12 CONE REYNOLDS NUMBER R_{ci}	13 INVISCID DRAG COEFFICIENT C_{Di}	14 SHEAR-DRAG COEFFICIENT (THEORETICAL) C'_{Df}
413	668.4	335.2	374.8	1.71	1780	0.2036	0.1501
	535.1		300.0		1425		0.1678
	409.6		229.7		1091		0.1917
	282.5		158.4		752		0.2309
	134.3		75.3		358		0.3349
421	640.1	335.2	358.9	1.71	852	0.2036	0.2169
	507.6		284.6		676		0.2436
	394.2		221.1		525		0.2764
	272.1		152.6		362		0.3327
	131.2		73.5		175		0.4793
414	1623	173.4	407.6	3.20	9532	0.1619	0.0968
	1262		317.0		7413		0.1098
	957.5		240.5		5624		0.1261
	747.6		187.8		4392		0.1427
	422.2		106.1		2481		0.1898
422	1648	173.4	413.8	3.20	4839	0.1619	0.1359
	1264		317.6		3714		0.1551
	957.7		240.5		2812		0.1783
	736.5		185.0		2163		0.2033
	419.4		105.3		1231		0.2695

TABLE II - Continued

DATA CORRECTED TO MACH NUMBER OF 2 AND 4

RUN NUMBER	15 TANGENT-CONE PRESSURE PARAMETER f	16 VISCOUS PRESSURE-DRAG COEFFICIENT (THEORETICAL) $C'_{Dp} - C_{Di}$	17 VISCOUS DRAG COEFFICIENT (THEORETICAL) $C'_D - C_{Di}$	18 TOTAL DRAG COEFFICIENT (THEORETICAL) C'_D	19 VISCOUS DRAG COEFFICIENT $C_D - C_{Di}$	20 TOTAL DRAG COEFFICIENT C_D
413	3.53	0.0360	0.1861	0.3897	0.2213	0.4249
		0.0402	0.2080	0.4116	0.2568	0.4604
		0.0460	0.2377	0.4413	0.2959	0.4995
		0.0553	0.2862	0.4898	0.3642	0.5678
		0.0802	0.4151	0.6187	0.5438	0.7474
421	3.53	0.0520	0.2689	0.4725	0.3109	0.5145
		0.0584	0.3020	0.5056	0.3811	0.5847
		0.0663	0.3427	0.5463	0.4198	0.6234
		0.0798	0.4125	0.6161	0.5184	0.7220
		0.1149	0.5942	0.7978	0.7758	0.9794
414	11.8	0.0277	0.1245	0.2864	0.1381	0.3000
		0.0314	0.1412	0.3031	0.1606	0.3225
		0.0361	0.1622	0.3241	0.1834	0.3453
		0.0409	0.1836	0.3455	0.2105	0.3724
		0.0544	0.2442	0.4061	0.2882	0.4501
422	11.8	0.0389	0.1748	0.3367	0.2012	0.3631
		0.0444	0.1995	0.3614	0.2396	0.4015
		0.0511	0.2294	0.3913	0.2724	0.4343
		0.0582	0.2615	0.4234	0.3100	0.4719
		0.0772	0.3467	0.5086	0.4146	0.5765

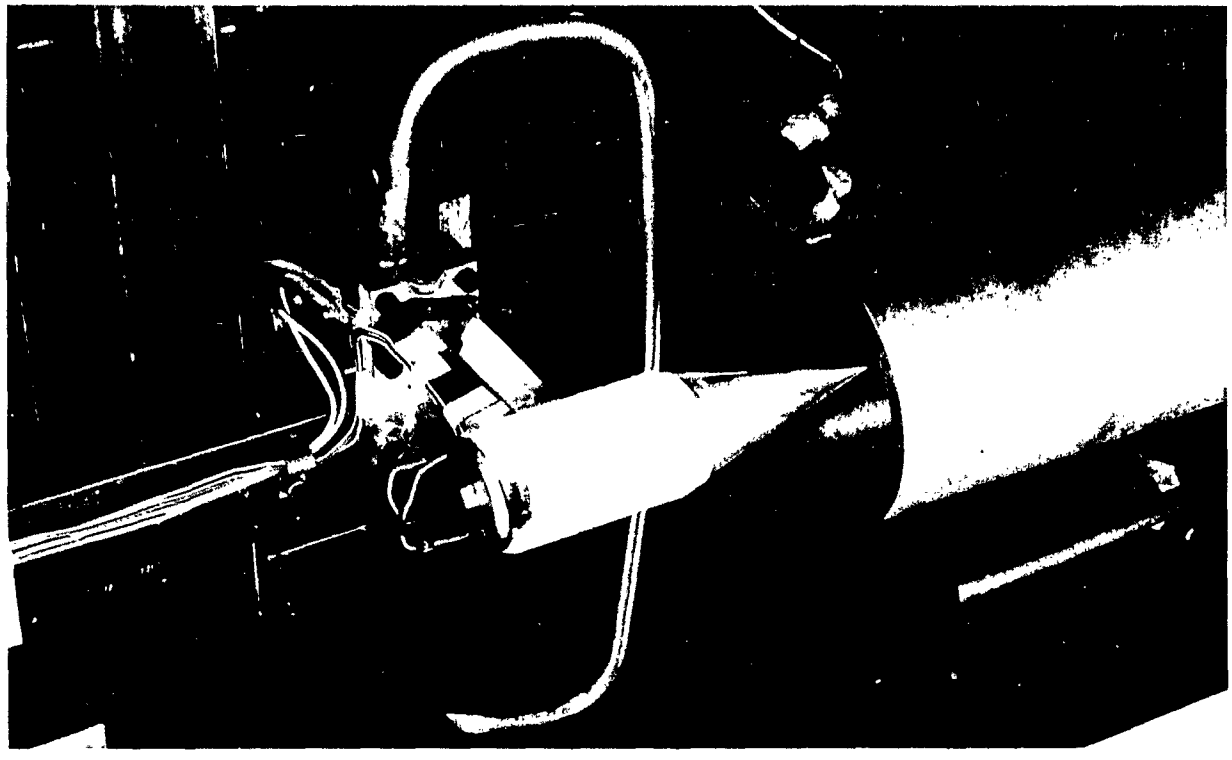

FIG. 1

ONE-INCH MODEL IN POSITION IN MACH 4 NOZZLE

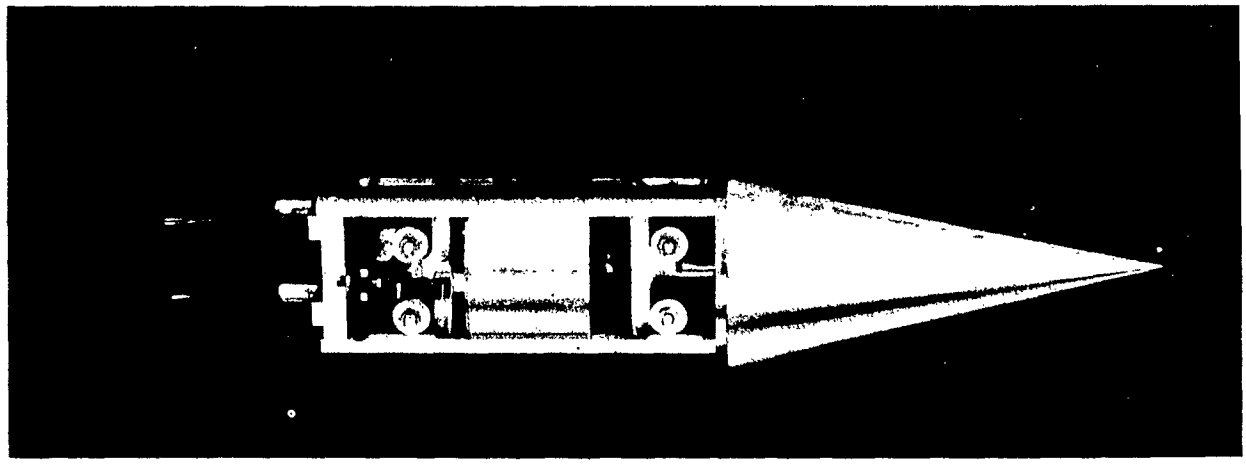

FIG. 2

VIEW WITH BALANCE REMOVED FROM HOUSING
(ONE-INCH MODEL)

PHOTO 240

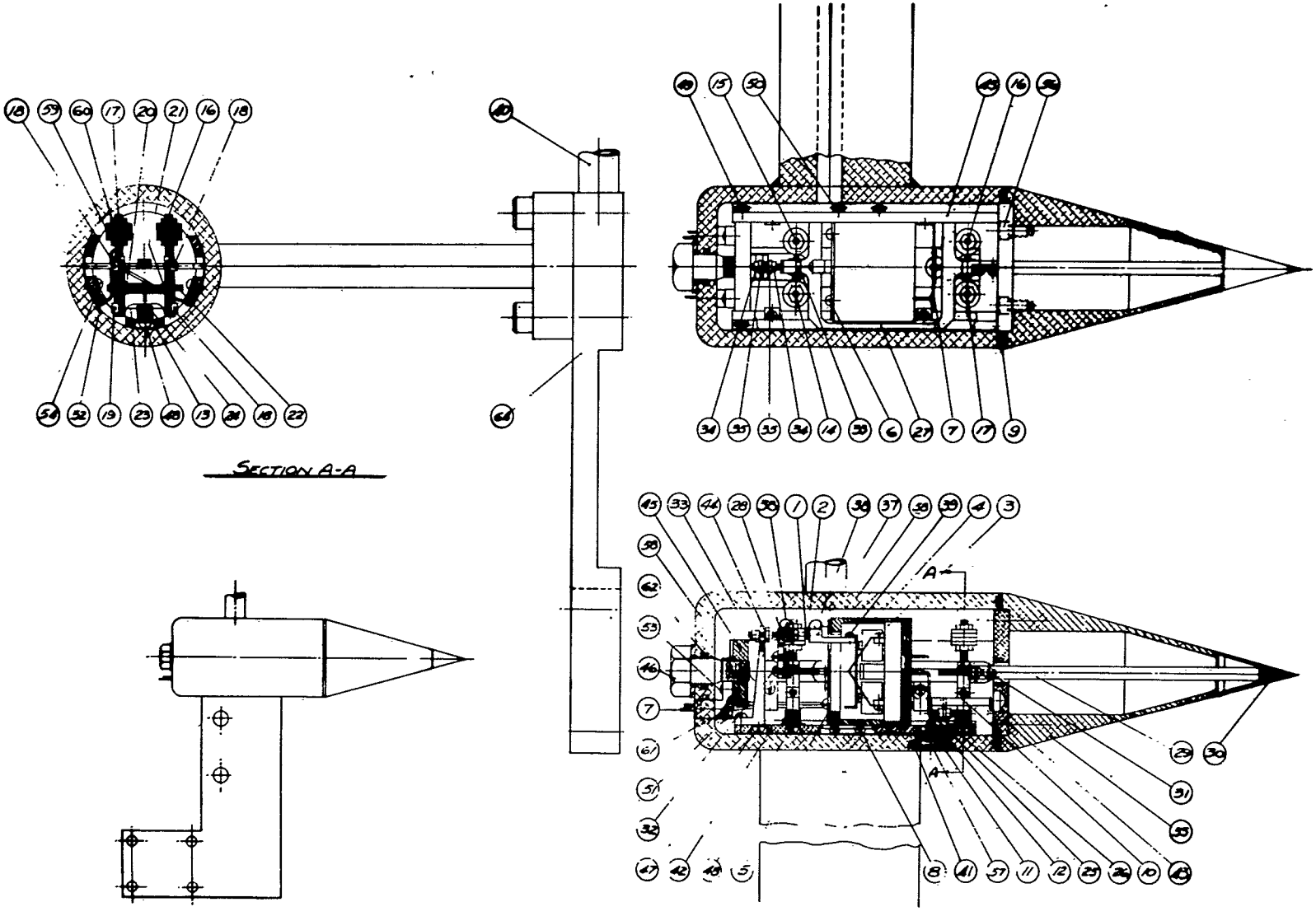

HYD 6520-150-0

FIG. 3 ASSEMBLY DRAWING OF BALANCE

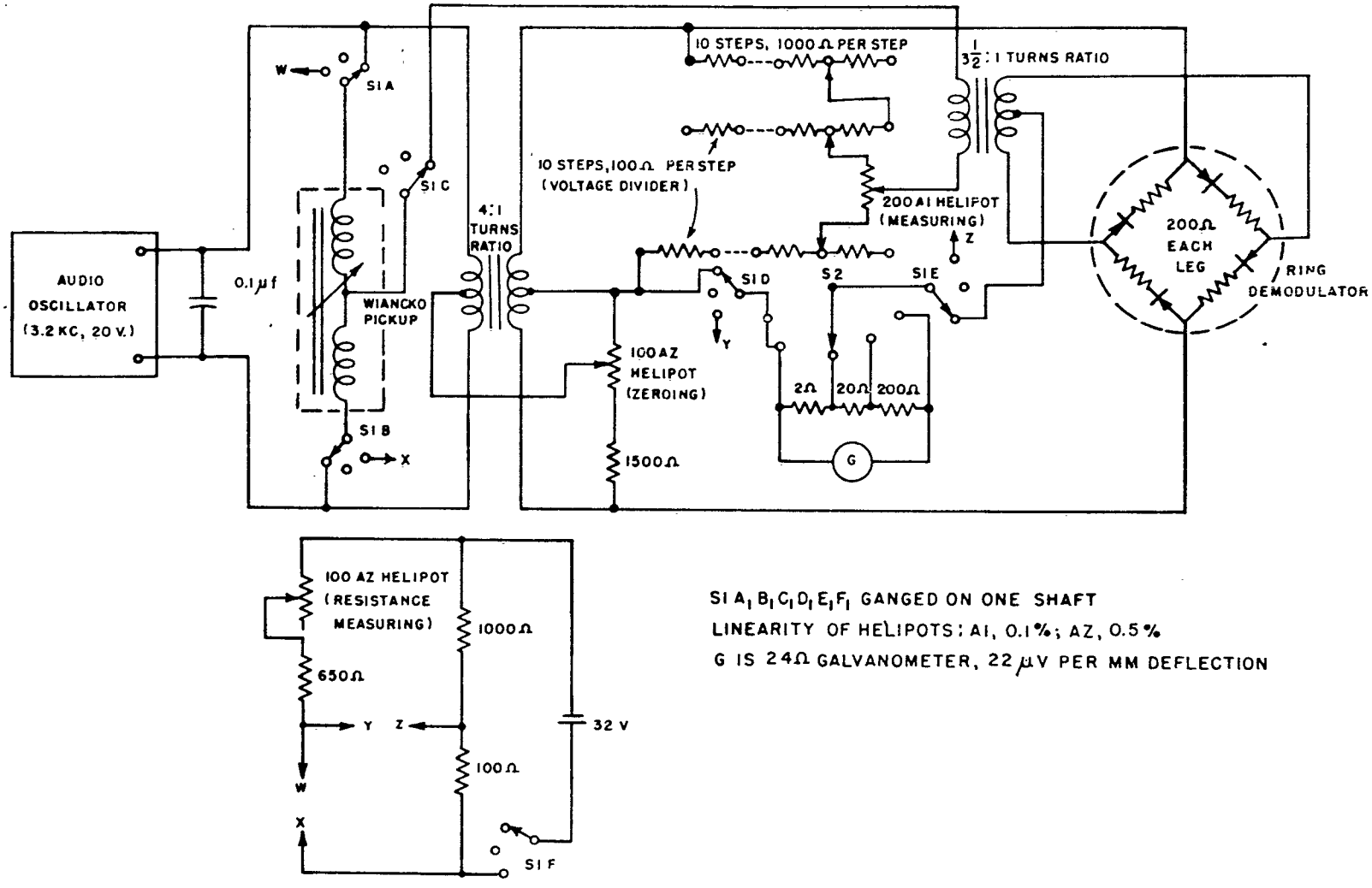

S1 $A_1 B_1 C_1 D_1 E_1 F_1$ GANGED ON ONE SHAFT
LINEARITY OF HELIPOTS: A1, 0.1%; A2, 0.5%
G IS 24Ω GALVANOMETER, 22 μV PER MM DEFLECTION

FIG. 4 MEASURING CIRCUIT

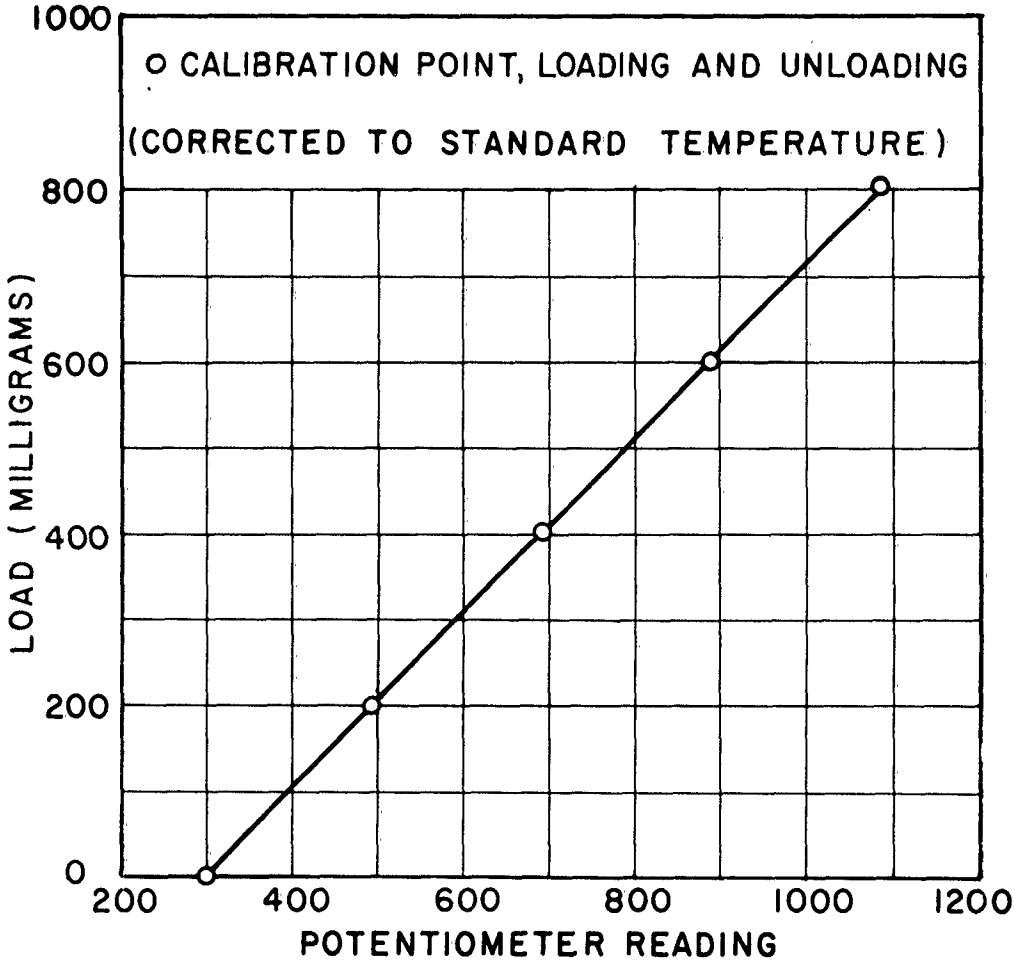

FIG.5 TYPICAL CALIBRATION OF WIANCKO UNIT

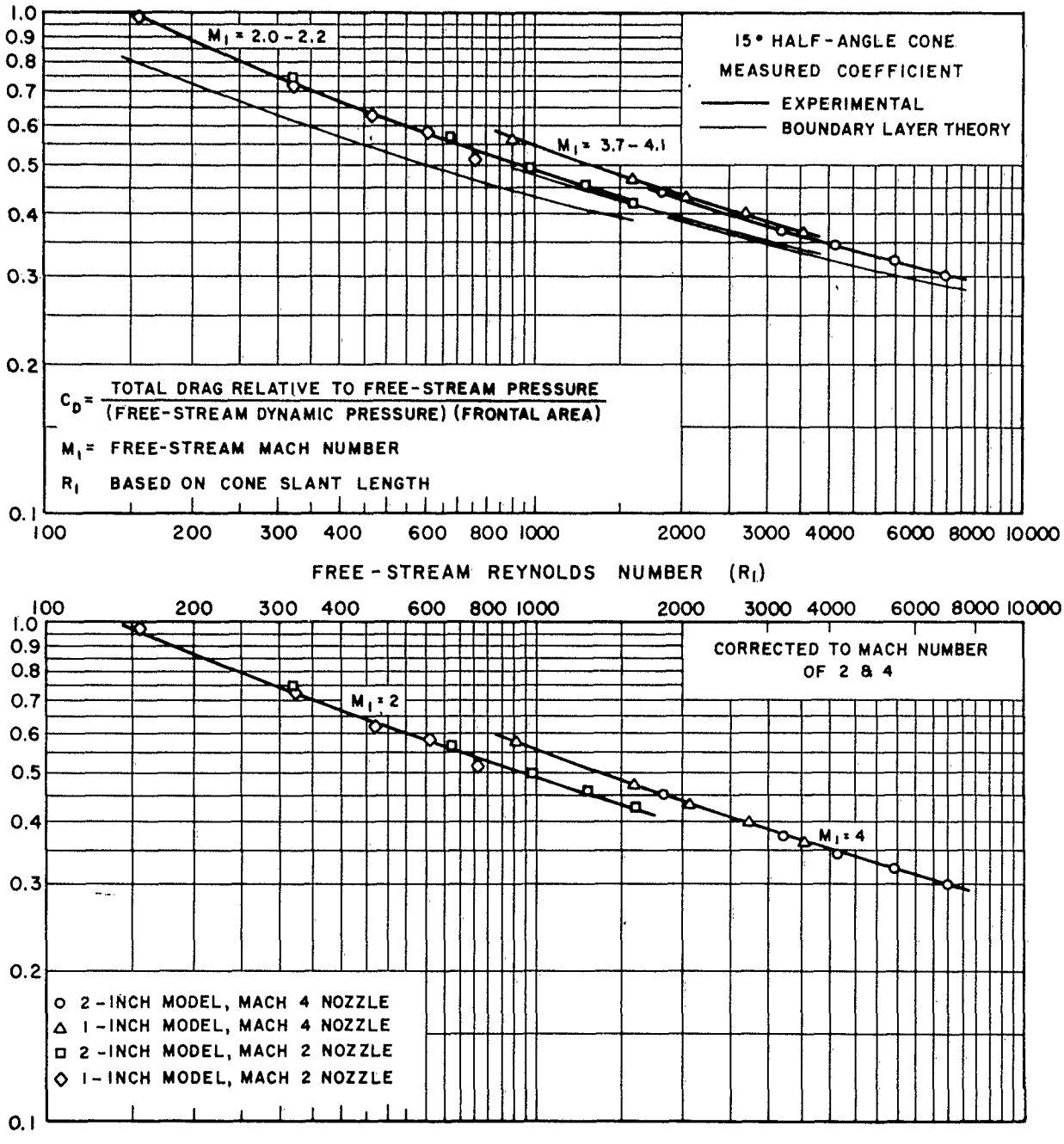

FIG. 6 TOTAL DRAG COEFFICIENT (C_D)

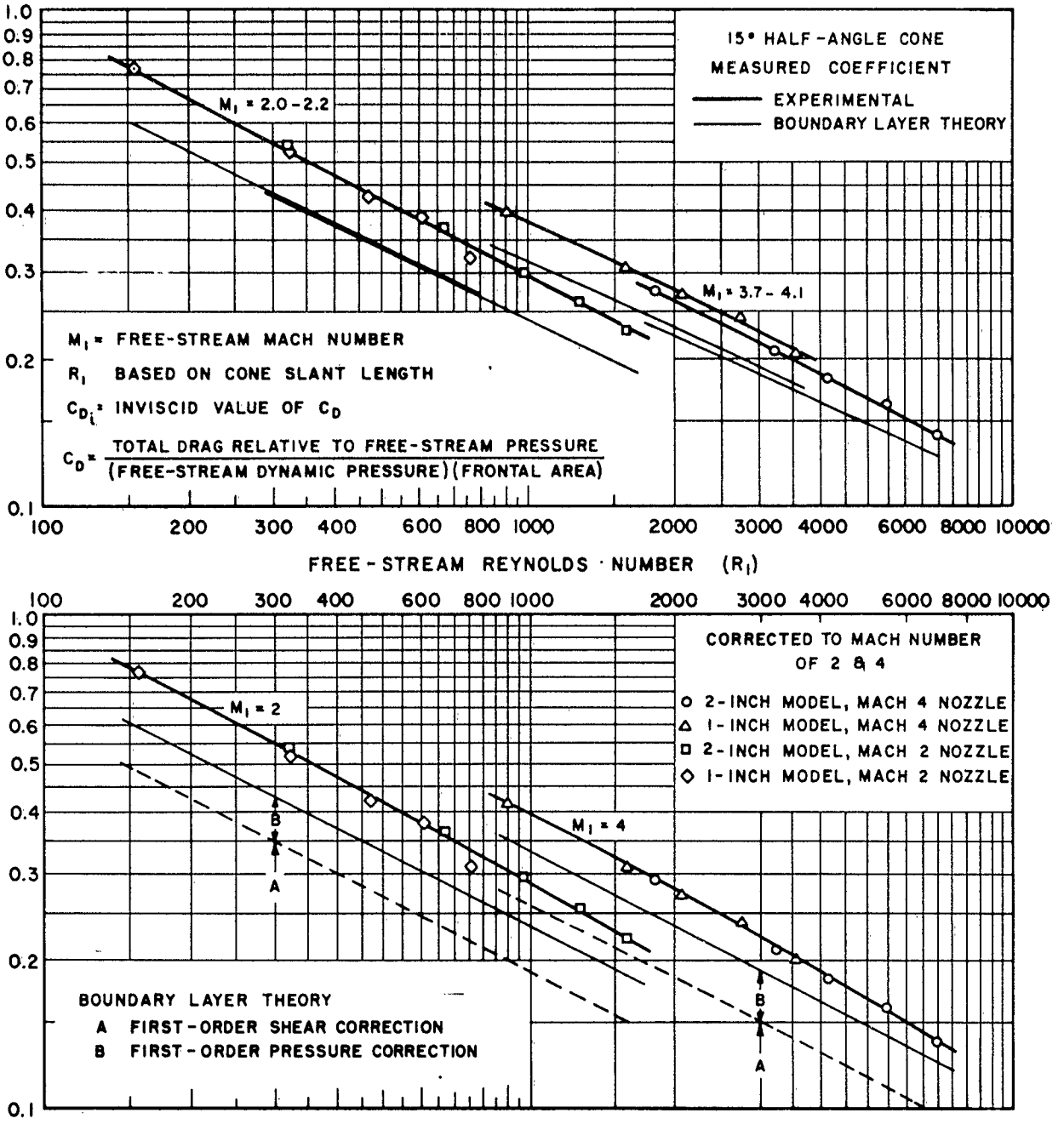

FIG. 7 VISCOUS DRAG COEFFICIENT ($C_D - C_{D_i}$)

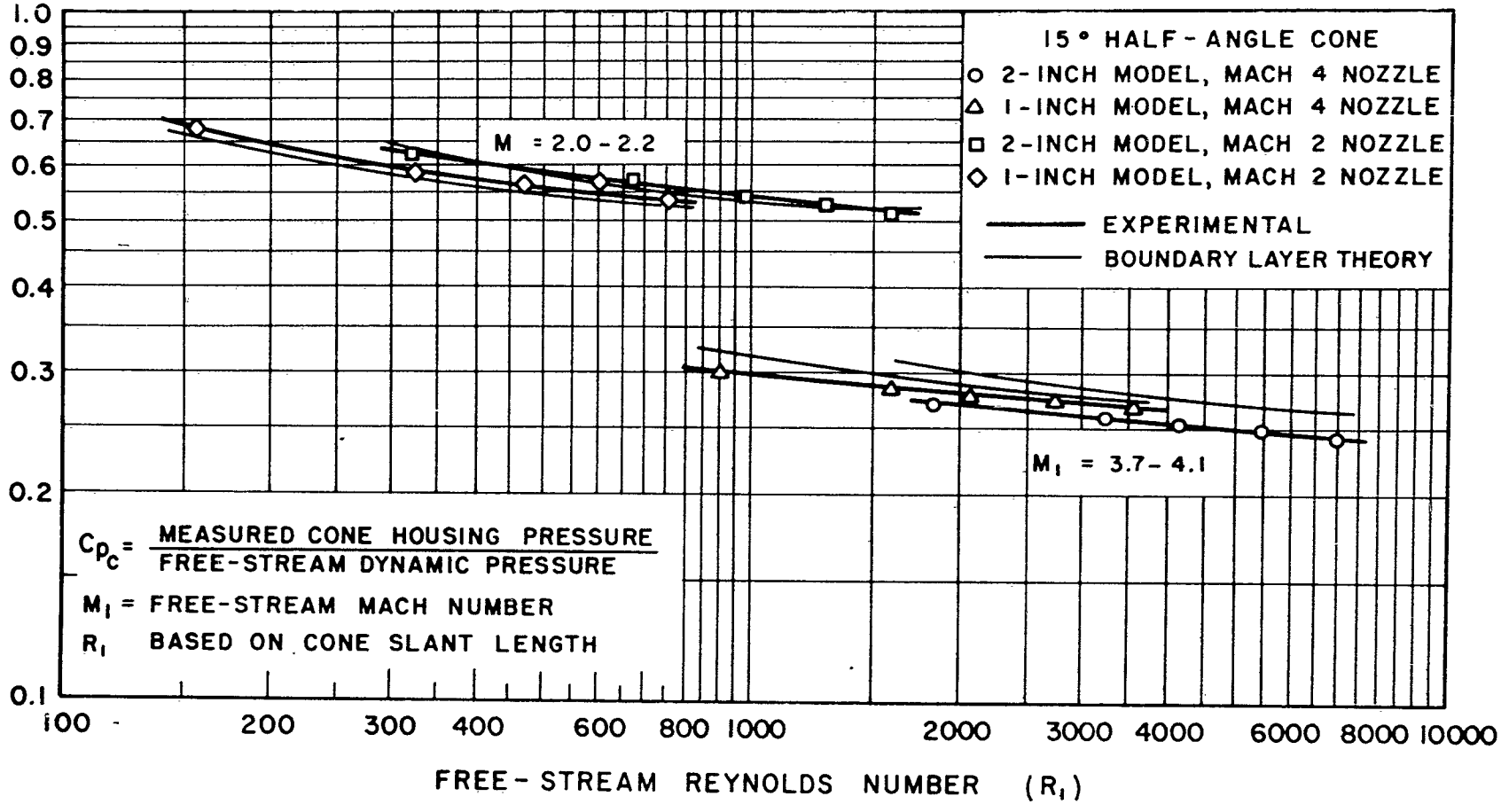

FIG. 8 MEASURED PRESSURE COEFFICIENT (C_{p_c})

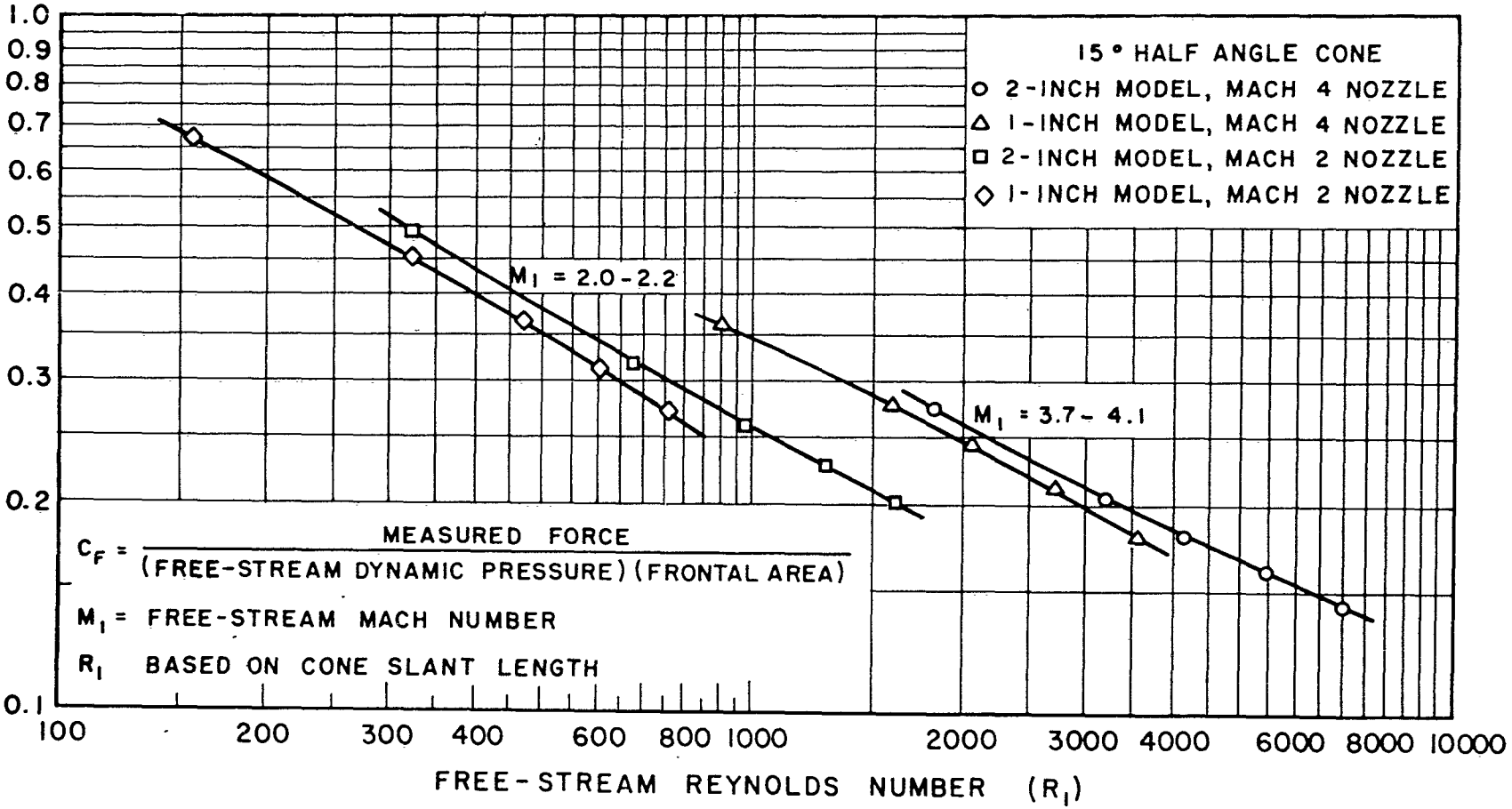

FIG. 9 MEASURED FORCE COEFFICIENT (C_F)

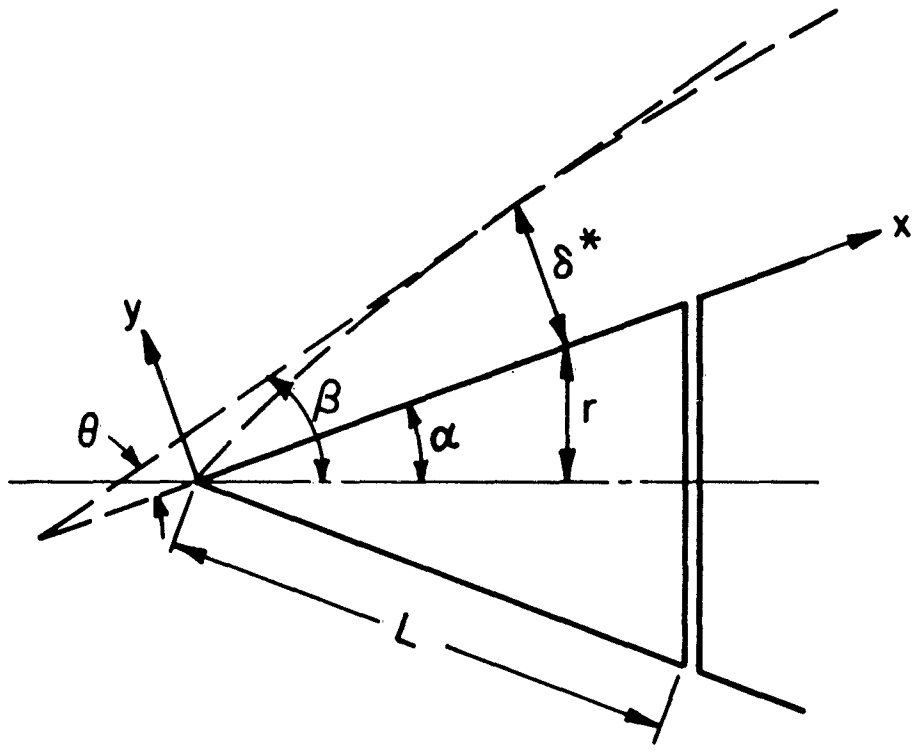

FIG. 10 CONE BOUNDARY-LAYER GEOMETRY

DISTRIBUTION LIST FOR ONR TECHNICAL REPORTS

Director, Aeronautical Research, NACA, 1724 F St. N.W., Wash. 25, D. C. (1)

Commanding General, Air Research and Development Command, P.O. Box 1395, Baltimore, Maryland - Attn: OSR(RDRF) (2)

Dr. Morton Alperin, Western Regional Office, Hdqrs., Air Research and Development Command, P.O. Box 2035, Pasadena 2, Calif. (1)

Director, Ames Aeronautical Lab., NACA, Moffett Field, Calif. (1)

Applied Physics Lab., Johns Hopkins Univ., 8621 Georgia Ave., Silver Spring, Md. (1)

Armed Forces Special Weapons Project, The Pentagon, Wash. 25, D. C. (1)

Commanding Officer, Arnold Engr. Development Center, Tullahoma, Tenn. - Attn: ACGT & ACR (1)

Mr. C. K. Bauer, Hermes Project, General Electric Co., Schenectady 5, N. Y. (1)

Prof. W. S. Bradfield, Dept. of Aeronautical Engr., Univ. of Minnesota, Minneapolis, Minnesota (1)

Chief, Bureau of Aeronautics, Dept. of the Navy, Wash. 25, D. C. - Attn: Aero and Hydro Branch (1)

Chief, Bureau of Aeronautics, Dept. of the Navy, Wash. 25, D. C. - Attn: Research Division (1)

Chief, Bureau of Ordnance, Dept. of the Navy, Wash. 25, D. C. - Attn: Re9a (1)

Dr. Francis H. Clauser, Johns Hopkins Univ., Dept. of Aeronautical Engr., Baltimore 18, Maryland (1)

Commanding Officer and Director, David Taylor Model Basin, Wash. 7, D. C. - Attn: Technical Library (1)

Chief of Naval Research, Dept. of the Navy, Wash. 25, D. C. - Attn: Code 438 (3)

Chief of Staff, Hdqrs USAF, Directorate of Research and Development, Wash. D. C. - Attn: AFDRD-AC2 (1)

Chief, Documents Service Center, Armed Services Technical Information Agency, U. B. Building, Dayton 2, Ohio (1 reproducible copy) (2)

Prof. Fred S. Eastman, Univ. of Wash., Dept. of Aeronautical Engr., Seattle 5, Wash. (1)

Dr. I. B. Esterman, Code 419, Office of Naval Research, Wash. D. C. (1)

Prof. K. O. Friedrichs, New York Univ., Institute for Mathematics and Mechanics, 45 Astor Place, New York, N. Y. (1)

Director, Jet Propulsion Lab., Calif. Institute of Technology, Pasadena, Calif. (1)

Dr. J. M. Jones, Engr. Research Institute, Univ. of Michigan, Ann Arbor, Mich. (1)

Prof. A. Kantrowitz, Graduate School of Aeronautical Engr., Cornell Univ., Ithaca, New York (1)

Dr. J. Kaplan, Dept. of Physics, Univ. of Calif. at Los Angeles, Los Angeles 24, Calif. (1)

Prof. J. H. Keenan, Massachusetts Institute of Technology, Mechanical Engr. Dept., Cambridge 39, Mass. (1)

Prof. M. Z. Krzywoblocki, Univ. of Illinois, Urbana, Illinois (1)

Dr. A. M. Kuethe, Dept. of Aeronautical Engr., Univ. of Michigan, Ann Arbor, Michigan (1)

Dr. A. R. Kuhlthau, Univ. of Virginia, Dept. of Physics, Charlottesville, Va. VIA: Naval Inspector of Ordnance, Applied Physics Lab., Johns Hopkins Univ., Silver Spring, Maryland (1)

Director, Langley Memorial Aeronautical Lab., NACA, Langley Field, Virginia (1)

Prof. Lester Lees, Aeronautical Engr. Dept., Princeton Univ., Princeton, N. J. (1)

Director, Lewis Flight Propulsion Laboratory, NACA, Cleveland, Ohio (1)

Prof. H. Lewy, Applied Mathematics Group, Stanford Univ., Stanford, Calif. (1)

Dr. James E. Lipp, The Rand Corp., 1500 Fourth St., Santa Monica, Calif. (1)

Dr. J. H. Marchant, Div. of Engr., Brown Univ., Providence 12, Rhode Island (1)

Prof. J. R. Markham, Mass. Institute of Technology, Cambridge 39, Mass. (1)

Dr. C. B. Millikan, Guggenheim Aeronautical Lab., Calif. Institute of Technology, Pasadena, Calif. (1)

Dr. Henry T. Nagamatsu, Director, Hypersonic Wind Tunnel, Calif. Institute of Technology, Pasadena 4, Calif. (1)

Commanding Officer, U. S. Naval Ordnance Test Station, Inyokern, China Lake Calif. - Attn: Technical Library (1)

Director, Naval Research Lab., Wash. 20, D. C. - Attn: Code 2020 (9)

Commander, Naval Ordnance Lab., White Oak, Silver Spring 19, Maryland - Attn: Aeroballistic Research Dept. (1)

Director, Office of Naval Research, 150 Causeway St., Boston, Mass. (1)

Director, Office of Naval Research, 346 Broadway, New York 13, N. Y. (1)

Director, Office of Naval Research, 844 North Rush St., Chicago 11, Illinois (1)

Director, Office of Naval Research, 1000 Geary St., San Francisco 9, Calif. (2)

Director, Office of Naval Research, 1030 East Green St., Pasadena 1, Calif. (1)

Officer in Charge, Office of Naval Research, Navy #100, Fleet Post Office New York, N. Y. (3)

Radiation Lab., Univ. of Calif., Berkeley 4, Calif. - Attn: R. Wakerling (1)

Chairman, Research and Development Board, The Pentagon, Wash. 25, D. C. - Attn: Information Requirement Board, Room 3D-1075 (1)

Mr. R. H. Shick, Consolidated Vultee Aircraft Corp., San Diego 12, Calif. (1)

Mr. Joseph Sternberg, Ballistics Research Lab., Ordnance Dept., Aberdeen, Md. (1)

Sverdrup and Parcel Inc., Consulting Engineers, Syndicate Trust Building, St. Louis, Missouri (1)

Dr. Theodore Theodorsen, Univ. of Maryland, Building J, Room 314, College Park, Maryland (1)

Dr. F. L. Wattendorf, Hdqrs. USAF, The Pentagon, Wash. 25, D. C. (1)

Western Coordination Office, NACA, 7660 Beverly Blvd., Los Angeles 36, Calif. (1)

Dr. E. P. Williams, Missiles Div., Rand Corp., 1500 Fourth St., Santa Monica, Calif. (1)

Wright Air Development Center, Wright-Patterson Air Force Base, Dayton, Ohio - Attn: WCRRS-3 (1) Attn: MCIDXE (1) (2)